ORIGINAL ARTICLE

Exploring facile synthesis and cholinesterase inhibiting potential of heteroaryl substituted imidazole derivatives for the treatment of Alzheimer's disease

Faryal Chaudhry [a,*], Rubina Munir [a], Muhammad Ashraf [b], Mehr-un-Nisa [c], Rahila Huma [a], Nayab Malik [a], Safdar Hussain [b], Munawar Ali Munawar [d,e,*], Misbahul Ain Khan [b,e]

[a] *Department of Chemistry, Kinnaird College for Women Lahore, 93-Jail Road, Lahore 54000, Pakistan*
[b] *Institute of Chemistry, The Islamia University of Bahawalpur, Bahawalpur 63100, Pakistan*
[c] *Department of Chemistry, The University of Lahore, Lahore, Pakistan*
[d] *School of Chemistry, University of the Punjab, Lahore 54590, Pakistan*
[e] *Department of Basic and Applied Chemistry, Faculty of Science and Technology, University of Central Punjab, Lahore, Pakistan*

Abstract Alzheimer's disease (AD) is a neurodegenerative disorder and cholinesterase (ChE) enzymes are considered as crucial targets for the treatment of AD. Herein, a series of heteroaryl substituted imidazole derivatives (**5a-5x**) was prepared using amino acid catalyzed, one-pot facile synthetic approach. In this context, the catalytic potentials of different amino acids were investigated and 15 mol% of glutamic acid was identified as the most suitable catalyst to obtain the target products in good yields up to 90 %. These structurally exciting heterocyclic hybrids were screened against acetylcholinesterase (AChE) and butyrylcholinesterase (BChE) enzymes. This series displayed moderate to excellent inhibitory potential against AChE with IC_{50} values > 25 μM and the most active compound was 3-(4-(1-(3,5-dimethylphenyl)-4,5-diphenyl-1*H*-imidazol-2-yl)-1-phenyl-1*H*-pyrazol-3-yl)–2*H*-chromen-2-one (**5x**) with IC_{50} value of 25.83 ± 0.25 μM.This inhibitory potential was attributed to hydrophobicity as the major contributory factor. The most potent compound against BChE was 1,3-diphenyl-4-(1,4,5-triphenyl-1*H*-imidazol-2-yl)-1*H*-pyrazole (**5a**) with IC_{50} value of 0.35 ± 0.02 μM followed by other potent compounds **5p, 5 m, 5x, 5b, 5c, 5e**

---

* Corresponding authors.
 E-mail addresses: faryal.chaudhry@kinnaird.edu.pk, frylchaudhry@yahoo.com (F. Chaudhry), munawarali@ucp.edu.pk (M. Ali Munawar).

and **5f** with IC$_{50}$ values < 10 μM. SAR studies further revealed that coumarinyl moiety at R^1 position in the imidazolylpyrazole skeleton significantly improved the overall cholinesterase inhibitory potential. However, a simple phenyl ring attached at this R^1 site was highly effective and selective for BChE inhibition (**5a**) over AChE. Docking data also demonstrated the interaction of **5x** and AChE with a docking score of 7564 and atomic contact energy (ACE) value of –291.90 kcal/mol whereas docking score for **5a** against BChE was 7096 with ACE value of –332.95 kcal/mol. The results altogether suggest further investigations of the heteroaryl substituted imidazole core skeleton in search of potential leads towards designing of new anti-cholinesterase drugs for the treatment of AD.

1. Introduction

Dementia is a neurodegenerative and a progressive cognitive impairment among the elderly people. This lethal syndrome has physical, psychological as well as social influences (Lott and Head 2019). Dementia is a 7th leading cause of mortality. Globally, more than 55 million people are struggling with the dementia per year. This estimate would be increased up to 132 million by the year of 2050 which is an alarming situation (Athar et al. 2021; Gaugler et al. 2022; Porsteinsson et al. 2021). Some of its universal forms have included: Alzheimer's disease (AD), vascular, Lewy bodies, frontotemporal dementia and Parkinson's disease. About 60–70 % of the dementia cases are associated with the AD. For many years, the AD was considered as a simple brain disorder. The generalized atrophy, β-amyloid plaques, and neurofibrillary tangles are some of the major AD pathological hallmarks. Scientists have envisaged etiology for the AD progression and also considered proteins as potential therapeutic targets (Cummings et al. 2022). Two forms of cholinesterases (ChEs); acetylcholinesterase (AChE, EC 3.1.1.7) and butyrylcholinesterase (BChE, EC 3.1.1.8), are engaged in regulating the acetylcholine levels which acts as neurotransmitter in a healthy brain. Sometimes this cholinergic disturbance causes substantial impact on cognition and could lead to neurodegeneration (Kabir et al. 2019). The structures of both enzymes are fairly similar; however, some differences have been observed in the sizes of their active site gorges which most probably affect the working approach of both ChEs (Chatonnet and Lockridge 1989; Jing et al. 2019; Rosenberry et al. 2017). So far, the most commonly prescribed formulations to treat AD are the anticholinesterase drugs such as Rivastigmine (Exelon®), Donepezil (Aricept®), Eserine (Antícholium®), Tacrine (Cognex®) and Galantamine (Razadyne®) (Grutzendler and Morris 2001; Kumari et al. 2022) (Fig. 1). The AChE was mainly targeted as key enzyme during AD treatment for a long time. As BChE activity is also enhanced in AD patients and associated with Aβ deposits, therefore, BChE inhibition is also suggested as a prudent curative approach towards minimizing the AD development (Darvesh 2016; Fernández-Bolaños and López 2022; Li et al. 2017b; Purgatorio et al. 2019).

Literature survey represents various N-heterocyclic scaffolds as the promising dual or highly selective inhibiting agents of ChE enzymes (Benazzouz-Touami et al. 2022; Derabli et al. 2018; Kumari et al. 2022; Li et al. 2021; Ma et al. 2020; Mlakić et al. 2022; Tariq et al. 2022; Tripathy et al. 2020). Imidazole is an example of N-heterocycle which constitutes many important biomolecules like histamine, purine, nucleic acid, and biotin etc. Medicinal chemists usually employ this easily ionizable N-heterocyclic moiety in improving the pharmacokinetics of lead molecules (Alghamdi et al. 2021). Due to its widespread applications, different imidazole and/or benzimidazole analogues are proposed as effective molecules that can deal with AD and other neurodegenerative disorders. A benzimidazole derivative - PQ912 was recently discovered as the most potent glutaminyl cyclase inhibitor and currently under Phase II trials in the patients of AD (Vijverberg et al 2021). Another analogue of benzimidazole has displayed excellent activity against a different target enzyme: C-jun N-terminal kinase (Jun et al. 2021; Qin et al. 2022). A biphenyl linked imidazole derivative was also proposed as a promising inhibitor of glutaminyl cyclase (Li et al. 2017a). Recent discoveries have highlighted the imidazole based templates as ChEs inhibitors also (Almansour et al. 2020; da Costa et al. 2013; Dhingra et al 2022; Karlsson et al. 2012; Kuzu et al. 2019; Obaid et al. 2022; Ramrao et al. 2021; Sari et al. 2022) (Fig. 1).

There are limited clinical options of medications to treat AD. The rapid increase in the drug resistance and different side effects associated with some of the existing clinical drugs underline the need to design and prepare new and more potent ChEs inhibitors for the better treatment of AD. The pivotal role of imidazoles in the prior literature has motivated us to design current research study. In this context, an imidazole based core skeleton of the targeted molecules was prepared through a facile and an efficient synthetic approach. So far, different catalysts have been reported in the literature to prepare imidazole derivatives *via* one-pot multi-component reaction (MCR) (Nguyen et al. 2019; Rossi et al. 2019; Takeda et al. 2022). Amino acids and their derivatives are among those promising versatile organocatalysts that could promote handy, facile and expedient transformations of precursors in to various heterocycles (Kaur et al. 2022; Vachan et al. 2020). Thus, the utility of amino acids in the preparation of heteroaryl imidazoles was explored in the present study through a model preparation of a derivative **5a**. The scope of current strategic methodology is further increased in delivering versatility by preparing other N-substituted imidazoles (**5b-5x**). Furthermore, all of these synthesized derivatives were evaluated against both ChEs to find out inhibiting potential of these molecules. The most potent compounds of the series could be further investigated as "lead" molecules towards designing of new drugs for better AD treatment.

2. Materials and methods

2.1. Chemicals and physical measurements

Chemicals and reagents of Sigma-Aldrich were purchased from commercial sources. TLC was performed over aluminum supported sheets of DC-Alufolien Silica Gel 60, F$_{254}$ Merck. For the determination of melting points, Gallen Kamp apparatus was used. FTIR spectra were recorded in Agilent Technologies Cary 630 FTIR spectrophotometer. After dissolving compounds in CDCl$_3$ solvent, their ^{1}H (^{13}C) NMR spectra were acquired either on MHz Bruker DPX Instruments of 300 (75), 500 (125) or on 700 (175) MHz with the coupling constant (J) in Hz. Mass spectra of the samples were recorded on GC MS DFS-Thermo and for elemental analyses; Perkin Elmer 2400 Series II CHN/S Analyzer was used. Pyrazole-4-carbaldehydes (**1a-1g**) were prepared by following conventional formylation protocol (Abdel-Wahab et al. 2011).
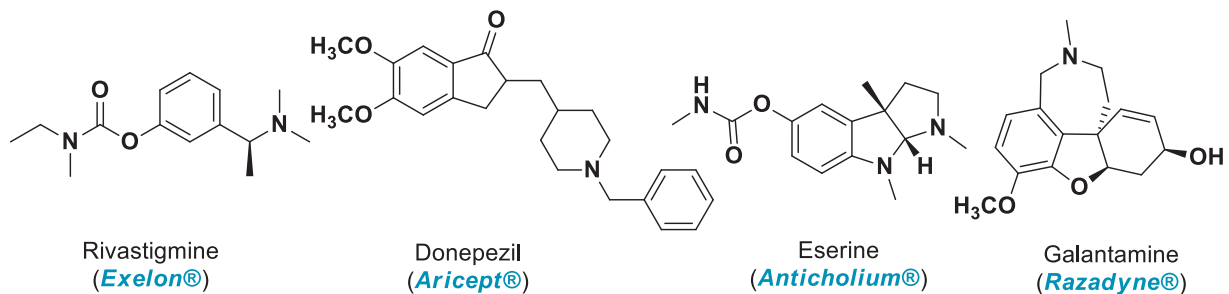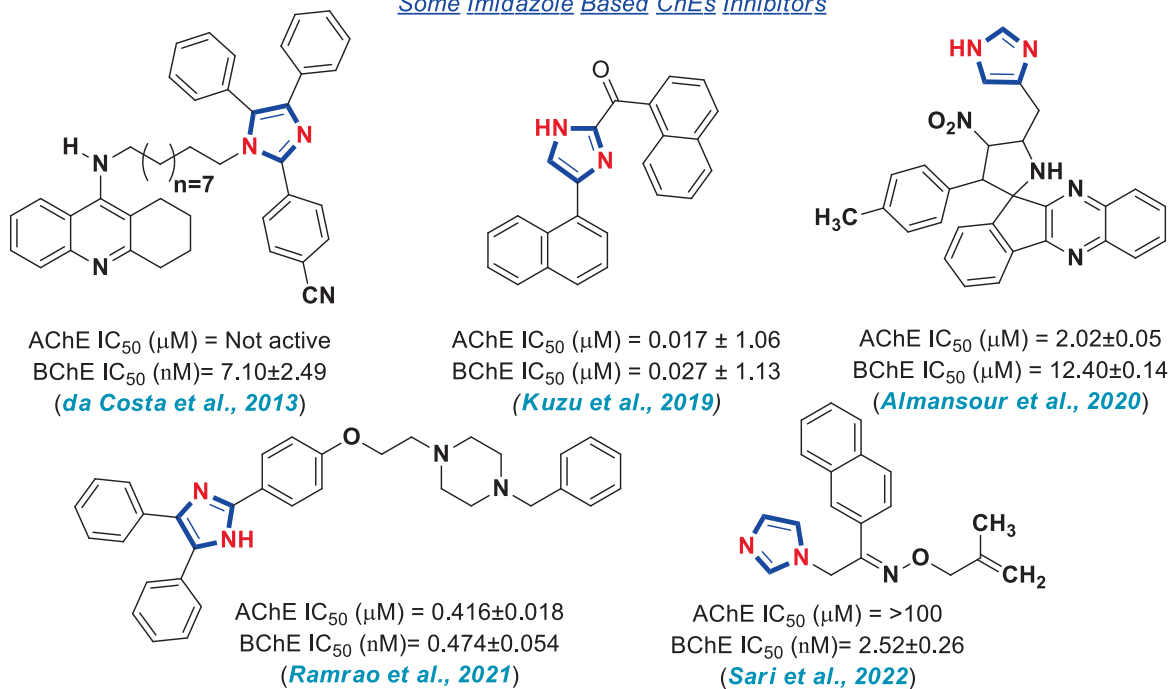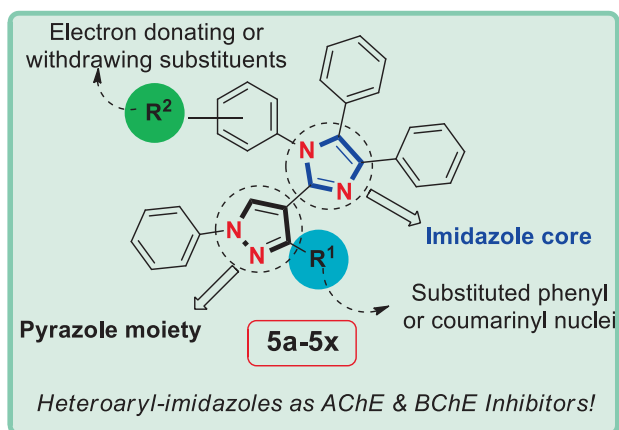
Fig. 1 Significant clinical drugs of AD and imidazole based potent anti-cholinesterase agents as rationale of the present study.

2.2. General synthetic protocol of heteroaryl-imidazoles (5a-5x)

A mixture of the corresponding aldehyde (1a-1g) (2.0 mmol, 1.0 equiv), substituted aniline (2a-2f) (2.0 mmol, 1.0 equiv), benzil (3) (2.0 mmol, 1.0 equiv), ammonium acetate (4) (2.0 mmol, 1.0 equiv) and glutamic acid (15 mol%, 0.3 mmol, 0.15 equiv) in EtOH (10 mL) was heated under reflux till reaction completion. The reaction mixture was allowed to cool down to r.t. The solution was diluted with cold water with vigorous stirring to obtain the precipitates of the desired product (5a-5x) which were filtered off and later purified through recrystallization with EtOH. The formation of compounds 5a, 5b, and 5k-5x was confirmed by comparing with the already reported data (Chaudhry et al. 2017c; Chaudhry et al. 2019; Shirole et al. 2017). Characterization data of the novel derivatives (5c-5j) are given below.

2.2.1. 4-(1-(4-Bromophenyl)-4,5-diphenyl-1H-imidazol-2-yl)-1,3-diphenyl-1H-pyrazole (5c)

Yield 72 % as white powder; m.p. 180–182 °C; IR (neat, v_{max}-cm^{-1}): 3137–3049 (C—H), 1596 (C=N), 1578 (C=C); ^{1}H NMR (500 MHz, CDCl$_3$) δ/ppm 6.33 (d, 2H, J = 8.5 Hz; Ar^3-2H), 6.97 (d, 2H, J = 8.5 Hz; Ar^3-2H), 7.09 (d, 2H, J = 6.5 Hz; Ar^4-2H), 7.21–7.24 (m, 6H; Ar^1-1H, Ar^2-3H, Ar^4-1H & Ar^5-1H), 7.27–7.34 (m, 6H; Ar^2-2H, Ar^4-2H & Ar^5-2H), 7.48 (t, 2H, J = 7.9 Hz; Ar^1-2H), 7.64 (d, 2H, J = 7.3 Hz; Ar^5-2H), 7.77 (d, 2H, J = 7.8 Hz; Ar^1-2H), 8.34 (s, 1H; H-5 Py); ^{13}C NMR (125 MHz, CDCl$_3$) δ/ppm 112.19 (C-4 Py), 119.11, 121.54 (C-Br), 126.94, 126.96, 127.44, 127.80, 128.17, 128.32, 128.33, 128.37, 128.70, 129.16, 129.52, 129.65, 130.09 (CH-5 Py), 130.35 (C-4' Im), 131.03, 131.41, 132.84, 134.24, 134.93, 138.52 (C-5' Im), 139.73, 140.55 (C-2' Im), 152.09 (C-3 Py); MS (EI+); m/z (%), 592.0 (M$^+$, 89.1), 594.1 ([M + 2]$^+$, 90.2); Anal. Calcd. for C$_{36}$H$_{25}$BrN$_4$; C, 72.85; H, 4.25; N, 9.44 %. Found: C, 72.69; H, 4.18; N, 9.35 %.

2.2.2. 4-(1-(4-Methoxyphenyl)-4,5-diphenyl-1H-imidazol-2-yl)-1,3-diphenyl-1H-pyrazole (5d)

Yield 80 % as purple powder; m.p. 156–158 °C; IR (neat, v_{max}-cm^{-1}): 3053–2844 (C—H), 1601 (C=N), 1591 (C=C), 1249 & 1026 (Ar^3-O-CH$_3$); ^{1}H NMR (500 MHz, CDCl$_3$) δ/ppm 3.68 (s, 3H; –OCH$_3$), 6.43 (d, 2H, J = 8.2 Hz; Ar^3-2H), 6.48 (d, 2H, J = 8.2 Hz; Ar^3-2H), 7.13–7.16 (m, 2H; Ar^4-2H), 7.24–7.34 (m, 10H; Ar^1-1H, Ar^2-3H, Ar^4-3H & Ar^5-3H), 7.42–7.45 (m, 2H, Ar^2-2H), 7.49 (t, 2H, J = 7.5 Hz; Ar^1-2H), 7.69 (d, 2H, J = 7.2 Hz; Ar^5-2H), 7.78 (d, 2H, J = 7.5 Hz; Ar^1-2H), 8.27 (s, 1H; H-5 Py); ^{13}C NMR (125 MHz, CDCl$_3$) δ/ppm 55.36 (–OCH$_3$), 112.38 (C-4 Py), 113.51, 119.05, 126.72, 126.78, 127.37, 127.81, 127.80, 128.03, 128.06, 128.25, 128.30, 128.48, 128.75, 128.82, 129.46 (CH-5 Py), 129.58, 130.61 (C-4' Im), 130.75, 131.05, 132.97, 137.93 (C-5' Im), 139.79, 140.79 (C-2' Im), 152.19 (C-3 Py), 158.56 (C-OCH$_3$); MS (EI+); m/z (%), 544.5 (M$^+$, 100); Anal. Calcd. for C$_{37}$H$_{28}$N$_4$O; C, 81.59; H, 5.18; N, 10.29 %. Found: C, 81.47; H, 5.10; N, 10.32 %.

2.2.3. 4-(1-(3,5-Dimethylphenyl)-4,5-diphenyl-1H-imidazol-2-yl)-1,3-diphenyl-1H-pyrazole (5e)

Yield 71 % as white powder; m.p. 102–104 °C; IR (neat, v_{max}-cm^{-1}): 3064–2918 (C—H), 1598 (C=N), 1561 (C=C);

^{1}H NMR (500 MHz, CDCl$_3$) δ/ppm 1.94 (s, 6H; 2 × CH$_3$), 6.11 (s, 2H; Ar^3-2H), 6.63 (s, 1H; Ar^3-1H), 7.11–7.50 (m, 16H; Ar^1-3H, Ar^2-5H, Ar^4-5H & Ar^5-3H), 7.64 (dd, 2H, J = 8.2, 1.1 Hz; Ar^5-2H), 7.74 (d, 2H, J = 8.5 Hz; Ar^1-2H), 8.23 (s, 1H; H-5 Py); ^{13}C NMR (125 MHz, CDCl$_3$) δ/ppm 21.07 (2 × CH$_3$), 112.67 (C-4 Py), 119.15, 125.68, 126.67, 126.77, 127.39, 127.93, 127.96, 127.98, 128.28, 128.29, 128.37, 129.39 (CH-5 Py), 129.44, 129.60, 130.57 (C-4' Im), 130.87, 131.03, 132.99, 134.67, 135.79 (C-5' Im), 137.86 (2 × C-CH$_3$), 137.98, 139.91, 140.59 (C-2' Im), 152.42 (C-3 Py); MS (EI+); m/z (%), 542.5 (M$^+$, 100); Anal. Calcd. for C$_{38}$H$_{30}$N$_4$; C, 84.10; H, 5.57; N, 10.32 %. Found: C, 84.33; H, 5.65; N, 10.40 %.

2.2.4. 3-([1,1'-Biphenyl]-4-yl)-4-(1-(3-chlorophenyl)-4,5-diphenyl-1H-imidazol-2-yl)-1-phenyl-1H-pyrazole (5f)

Yield 77 % as white powder; m.p. 158–160 °C; IR (neat, v_{max}-cm^{-1}): 3050–3028 (C—H), 1595 (C=N), 1588 (C=C), 763 (C-Cl); ^{1}H NMR (500 MHz, CDCl$_3$) δ/ppm 6.42 (s, 1H; Ar^3-1H), 6.47 (d, 1H, J = 8.0 Hz; Ar^3-1H), 6.82 (t, 1H, J = 8.0 Hz; Ar^3-1H), 6.97 (d, 1H, J = 8.0 Hz; Ar^3-1H), 7.08 (d, 2H, J = 6.5 Hz; Ar^4-2H), 7.18–7.21 (m, 4H; Ar^2-1H & Ar^4-3H), 7.24–7.28 (t, 2H; Ar^2-2H), 7.29–7.33 (m, 2H; Ar^1-1H & Ar^5-1H), 7.36 (d, 2H, J = 8.0 Hz; Ar^2-2H), 7.41 (t, 2H, J = 7.5 Hz; Ar^5-2H), 7.45–7.48 (m, 4H; Ar^1-2H & Ar^2-2H), 7.57 (d, 2H, J = 7.5 Hz; Ar^5-2H), 7.62 (d, 2H, J = 7.5 Hz; Ar^1-2H), 7.75 (d, 2H, J = 8.0 Hz; Ar^2-2H), 8.31 (s, 1H; H-5 Py); ^{13}C NMR (75 MHz, CDCl$_3$) δ/ppm 111.54 (C-4 Py), 119.22, 126.03, 127.05, 127.21, 127.50, 127.98, 128.04, 128.11, 128.44, 128.55, 128.75, 128.88, 129.24, 129.67, 129.81, 129.91, 130.22, 130.97, 131.56 (C-4' Im), 133.85 (C-Cl), 136.46, 136.72, 137.88 (C-5' Im), 139.68, 140.43, 140.82, 141.11 (C-2' Im), 151.78 (C-3 Py); Anal. Calcd. for C$_{42}$H$_{29}$ClN$_4$; C, 80.69; H, 4.68; N, 8.96 %. Found: C, 80.78; H, 4.76; N, 9.15 %.

2.2.5. 3-([1,1'-Biphenyl]-4-yl)-4-(1-(4-chlorophenyl)-4,5-diphenyl-1H-imidazol-2-yl)-1-phenyl-1H-pyrazole (5 g)

Yield 75 % as white powder; m.p. 200–202 °C; IR (neat, v_{max}-cm^{-1}): 3066–3028 (C—H), 1598 (C=N), 1577 (C=C), 764 (C-Cl); ^{1}H NMR (700 MHz, CDCl$_3$) δ/ppm 6.45 (d, 2H, J = 8.4 Hz; Ar^3-2H), 6.83 (d, 2H, J = 8.4 Hz; Ar^3-2H), 7.10 (d, 2H, J = 6.9 Hz; Ar^4-2H), 7.21–7.26 (m, 4H; Ar^2-1H & Ar^4-3H), 7.29 (t, 2H, J = 7.7 Hz; Ar^2-2H), 7.33 (t, 1H, J = 7.7 Hz; Ar^5-1H), 7.35–7.37 (m, 3H; Ar^1-1H & Ar^2-2H), 7.45 (t, 2H, J = 7.7 Hz; Ar^5-2H), 7.46–7.50 (m, 4H; Ar^1-2H & Ar^2-2H), 7.59 (d, 2H, J = 7.7 Hz; Ar^5-2H), 7.66 (d, 2H, J = 7.6 Hz; Ar^1-2H), 7.79 (d, 2H, J = 7.9 Hz; Ar^2-2H), 8.38 (s, 1H; H-5 Py); ^{13}C NMR (175 MHz, CDCl$_3$) δ/ppm 112.13 (C-4 Py), 119.09, 126.97, 127.00, 127.09, 127.46, 127.56, 128.22, 128.33, 128.39, 128.41, 128.71, 128.90, 128.99, 129.66, 130.11 (C-4' Im), 130.22, 131.00, 131.84, 133.50 (C-Cl), 134.08, 134.37, 138.41 (C-5' Im), 139.69, 140.53, 140.83, 140.95 (C-2' Im), 151.64 (C-3 Py); MS (EI+); m/z (%), 624.7 (M$^+$, 100), 626.5 ([M + 2]$^+$ 39.8); Anal. Calcd. for C$_{42}$H$_{29}$ClN$_4$; C, 80.69; H, 4.68; N, 8.96 %. Found: C, 80.77; H, 4.75; N, 9.01 %.

2.2.6. 3-([1,1'-Biphenyl]-4-yl)-4-(1-(4-bromophenyl)-4,5-diphenyl-1H-imidazol-2-yl)-1-phenyl-1H-pyrazole (5 h)

Yield 78 % as white powder; m.p. 218–220 °C; IR (neat, v_{max}-cm^{-1}): 3064–3028 (C—H), 1598 (C=N), 1561 (C=C);

^{1}H NMR (500 MHz, CDCl$_3$) δ/ppm 6.37 (d, 2H, J = 8.5 Hz; Ar^3-2H), 6.97 (d, 2H, J = 8.5 Hz; Ar^3-2H), 7.09 (dd, 2H, J = 7.5, 1.2 Hz; Ar^4-2H), 7.20–7.26 (m, 4H; Ar^2-1H & Ar^4-3H), 7.29 (t, 2H, J = 7.5 Hz; Ar^2-2H), 7.31–7.34 (m, 3H; Ar^2-2H & Ar^5-1H), 7.36–7.37 (m, 1H; Ar^1-1H), 7.44–7.51 (m, 6H; Ar^1-2H, Ar^2-2H & Ar^5-2H), 7.60 (d, 2H, J = 7.4 Hz; Ar^5-2H), 7.65 (d, 2H, J = 7.4 Hz; Ar^1-2H), 7.79 (d, 2H, J = 7.9 Hz; Ar^2-2H), 8.41 (s, 1H; H-5 Py); ^{13}C NMR (125 MHz, CDCl$_3$) δ/ppm 112.15 (C-4 Py), 119.08, 121.63 (C-Br), 126.97, 127.10, 127.47, 127.56, 128.24, 128.34, 128.29, 128.72, 128.99, 129.19, 129.67, 130.01 (C-4′ Im), 130.19, 131.00, 131.37, 131.83, 134.07, 134.09, 134.86, 138.45 (C-5′ Im), 139.69, 140.48, 140.84, 140.94 (C-2′ Im), 151.64 (C-3 Py); MS (EI+); m/z (%), 668.0 (M$^+$, 84.1), 670.0 ([M + 2]$^+$, 88.2); Anal. Calcd. for C$_{42}$H$_{29}$BrN$_4$; C, 75.33; H, 4.37; N, 8.37 %. Found: C, 74.20; H, 4.28; N, 8.46 %.

2.2.7. 3-([1,1′-Biphenyl]-4-yl)-4-(1-(4-methoxyphenyl)-4,5-diphenyl-1H-imidazol-2-yl)-1-phenyl-1H-pyrazole (5i)

Yield 82 % as purple powder; m.p. 186–187 °C; IR (neat, v_{max}-cm^{-1}): 3053–2972 (C—H), 1602 (C=N), 1578 (C=C), 1244 & 1024 (Ar^1-O-CH$_3$); ^{1}H NMR (500 MHz, CDCl$_3$) δ/ppm 3.63 (s, 3H; –OCH$_3$), 6.38 (d, 2H, J = 8.8 Hz; Ar^3-2H), 6.47 (d, 2H, J = 8.8 Hz; Ar^3-2H), 7.10 (dd, 2H, J = 7.8, 2.0 Hz; Ar^4-2H), 7.16–7.20 (m, 4H; Ar^2-1H & Ar^4-3H), 7.24–7.34 (m, 4H; Ar^1-1H, Ar^2-2H & Ar^5-1H), 7.40–7.47 (m, 8H; Ar^1-2H, Ar^2-4H & Ar^5-2H), 7.57 (d, 2H, J = 7.4 Hz; Ar^5-2H), 7.62 (d, 2H, J = 7.3 Hz; Ar^1-2H), 7.73 (d, 2H, J = 7.8 Hz; Ar^2-2H), 8.21 (s, 1H; H-5 Py); ^{13}C NMR (5 MHz, CDCl$_3$) δ/ppm 55.39 (–O$\underline{C}$H$_3$), 111.69 (C-4 Py), 113.53, 119.13, 126.92, 127.05, 127.50, 128.21, 128.39, 128.57, 128.80, 128.95, 129.63, 129.94, 130.29, 130.58, 131.05, 131.89 (C-4′ Im), 133.72, 137.35, 137.41 (C-5′ Im), 139.71, 140.65, 140.78, 140.86 (C-2′ Im), 151.75 (C-3 Py), 158.69 (-$\underline{C}$-OCH$_3$); MS (EI+); m/z (%), 620.6 (M$^+$, 100); Anal. Calcd. for C$_{43}$H$_{32}$N$_4$O; C, 83.20; H, 5.20; N, 9.03 %. Found: C, 83.09; H, 5.11; N, 8.90 %.

2.2.8. 3-([1,1′-Biphenyl]-4-yl)-4-(1-(3,5-dimethylphenyl)-4,5-diphenyl-1H-imidazol-2-yl)-1-phenyl-1H-pyrazole (5j)

Yield 73 % as light brown powder; m.p. 164–166 °C; IR (neat, v_{max}-cm^{-1}): 3127–2919 (C—H), 1598 (C=N), 1561 (C=C); ^{1}H NMR (700 MHz, CDCl$_3$) δ/ppm 1.93 (s, 6H; 2 × CH$_3$), 6.18 (s, 2H; Ar^3-2H), 6.64 (s, 1H; Ar^3-1H), 7.14 (dd, 2H, J = 6.6, 1.1 Hz; Ar^4-2H), 7.19–7.23 (m, 4H; Ar^2-1H & Ar^4-3H), 7.29 (t, 2H, J = 7.7 Hz; Ar^2-2H), 7.31 (t, 1H, J = 7.7 Hz; Ar^5-1H), 7.35 (t, 1H, J = 7.7 Hz; Ar^1-1H), 7.44 (t, 2H, J = 7.7 Hz; Ar^5-2H), 7.46–7.53 (m, 6H; Ar^1-2H & Ar^2-4H), 7.61 (d, 2H, J = 7.7 Hz; Ar^5-2H), 7.67 (d, 2H, J = 7.7 Hz; Ar^1-2H), 7.76 (d, 2H, J = 8.4 Hz; Ar^2-2H), 8.27 (s, 1H; H-5 Py); ^{13}C NMR (175 MHz, CDCl$_3$) δ/ppm 21.12 (2 × CH$_3$), 112.52 (C-4 Py), 119.15, 125.69, 126.74, 126.81, 126.91, 127.07, 127.42, 127.44, 128.02, 128.31, 128.32, 128.40, 128.92, 129.36 (CH-5 Py), 129.58, 129.62, 130.58 (C-4′ Im), 130.73, 131.01, 132.07, 134.49, 135.70 (C-5′ Im), 137.91 (2 × C-CH$_3$), 139.87, 140.54, 140.64, 140.87 (C-2′ Im), 151.97 (C-3 Py); MS (EI+); m/z (%), 618.6 (M$^+$, 100); Anal. Calcd. for C$_{44}$H$_{34}$N$_4$; C, 85.41; H, 5.54; N, 9.05 %. Found: C, 85.52; H, 5.46; N, 8.95 %.

2.3. Cholinesterase inhibition assay

Ellman's method with slight modification was used for the inhibition studies against AChE and BChE as reported earlier (Tariq et al. 2022). Total assay volume of 100 μL contained 60 μL of 50 mM phosphate buffer (pH 7.7), 10 μL of 0.5 mM test compounds (5a-5x) and 10 μL of 0.005 units of electric eel AChE enzyme (Sigma) or 0.0005 units equine serum BChE enzyme (Sigma). Reaction contents were pre-incubated at 37 °C for 10 min and pre-read at 405 nm using Synergy HTX BioTek 96-well plate reader. Reaction was started by the addition of 10 μL of substrate (acetylthiocholine iodide or butyrylcholine bromide), 10 μL of coloring reagent DTNB and incubation continued at 37 °C for 30 min. Contents were read at 405 nm and the percentage inhibition was calculated using following formula.

$$\text{Inhibition}\,(\%) = \left(\frac{\text{Abs of control} - \text{Abs of test compd.}}{\text{Abs of control}} \right) \times 100$$

All experiments were performed in triplicates with negative and positive controls. IC$_{50}$ values of the active compounds were determined by repeating assays with suitable dilutions of the test compounds and computing data using EZ-FIT software of Perrella Int., USA. Data is presented as Mean ± SEM, n = 3.
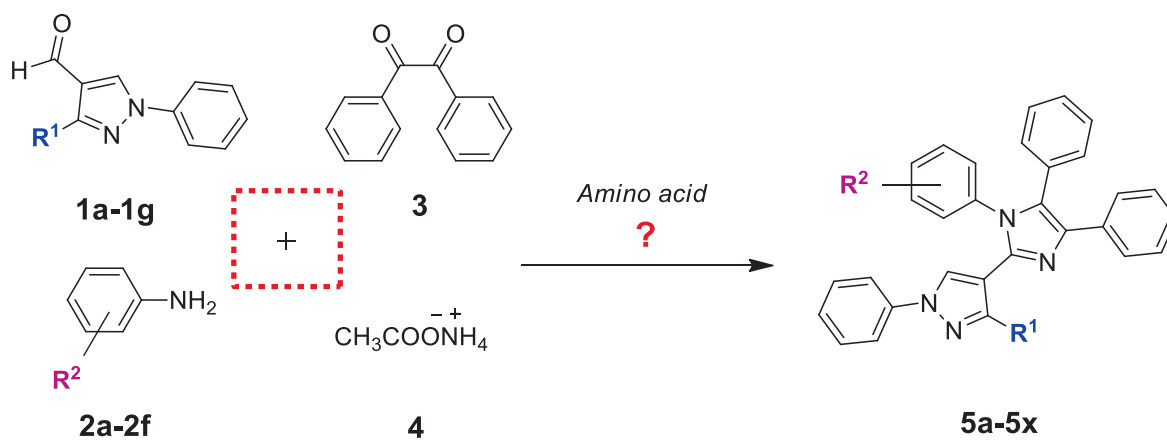
2.4. Molecular docking calculations

The crystal structures of AChE and BChE proteins were recovered from PDB (ID4M0E and 4BDS). The coordinate files were subjected to the Discovery Studio 4.5 Visualizer for pre-docking receptor formation by eliminating water molecules and incorporating hydrogen atoms. Compounds 5a-5x were docked with both the enzymes by *PatchDock* which is a molecular docking tool targeted to find docking transformations that produce good molecular shape complementarity (Schneidman-Duhovny et al. 2005). The input files comprised of the receptor protein and ligand in PDB format. *PatchDock* server afforded multiple solutions and the "solution 1" was selected as it surrounded the most significant amino acid residues as binding pouch for docking analyses assigned in crystal structure of AChE and BChE receptor (Cheung et al., 2013; Nachon et al. 2013). The docked complexes were observed *via* Discovery Studio 4.5 Visualizer. The binding affinities of the docked complexes were assessed as scores and ACE (atomic contact energy) of the docked structures. The hydrophobic and hydrogen bonding contacts of each ligand were evaluated inside the binding pouch of receptor protein.

3. Results and discussion

3.1. Chemistry

The convenience of MCR synthetic strategy and role of different catalysts in building of imidazole nucleus are acknowledged in the literature (Nguyen et al. 2019; Rossi et al. 2019; Takeda et al. 2022). Our research group has continuously been involved in finding better reaction conditions of imidazole synthesis (Chaudhry et al. 2017a; Chaudhry et al. 2017b; Naureen et al. 2017). Therefore, present work is another effort which

**Scheme 1**   Probing amino acid catalyzed synthesis of heteroaryl substituted imidazoles (**5a-5x**).

showed the expedient preparation of some aryl decorated imidazolylpyrazoles (**5a-5x**) (Scheme 1).

Catalytic utility of some amino acids was explored through a model reaction which was performed between the substrates: **1a**, **2a**, **3** and **4**. For preliminary screening of amino acids, six different amino acids were carefully selected for the investigation. Glycine, a simplest amino acid, was first explored on the basis of our previous findings (Chaudhry et al. 2017a; Naureen et al. 2017). The reaction has involved refluxing of the MCR mixture in EtOH along with glycine (15 mol%) as a catalyst. Proline is one such amino acid which had been used as a catalyst in the green synthesis of different heterocycles (Vachan

et al. 2020) and also gave better results in our present research study. Product **5a** was obtained in good yield by using aspartic acid or glutamic acid, probably the acidic catalysis enhances the reaction development. However, basic amino acids (lysine and histidine) gave moderate yield of the product even refluxing for 6 hrs. A catalyst-free reaction (Entry-7) did not result in good product yield.

The reaction was afterwards performed by loading different mole percentages (5–20 mol%) of the glutamic acid. The 5 mol % amount of catalyst resulted in 40 % product yield. The most suitable catalyst dose was screened out to be 15 mol% with 83 % product yield with in just 30 min reflux time, while,

Table 1   Optimization of the reaction conditions of a model reaction.
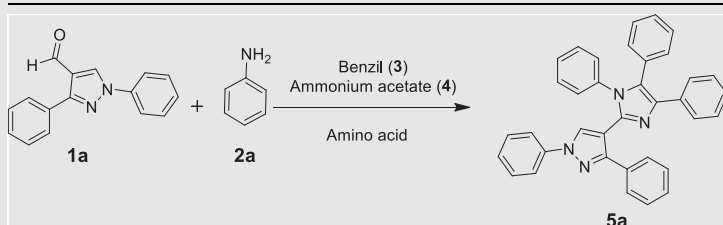
Entry	Catalyst (mol%)	Solvent (10 mL)/Condition	Time (min)	Yield (%)
1	Glycine (15)	EtOH/Reflux	60	80
2	Proline (15)	EtOH/Reflux	60	75
3	Aspartic acid (15)	EtOH/Reflux	30	80
4	**Glutamic acid (15)**[a]	**EtOH/Reflux**	**30**	**83**
5	Lysine (15)	EtOH/Reflux	360	33
6	Histidine (15)	EtOH/Reflux	360	30
7	–	EtOH/Reflux	360	< 20
8	Glutamic acid (15)	CH$_2$Cl$_2$/Reflux	60	32
9	Glutamic acid (15)	CH$_3$CN/Reflux	60	45
10	Glutamic acid (15)	MeOH/Reflux	30	78
11	Glutamic acid (15)	DMF/Heating at 100 °C	60	50
12	Glutamic acid (15)	DMSO/Heating at 100 °C	60	54
13	Glutamic acid (15)	H$_2$O/Reflux	120	75
14	Glutamic acid (5)	EtOH/Reflux	30	40
15	Glutamic acid (10)	EtOH/Reflux	30	54
16	Glutamic acid (20)	EtOH/Reflux	30	82

[a] Optimized reaction conditions.

Table 2 Preparation of aryl- and heteroaryl-decorated imidazoles[a] (**5a-5x**).

5a-5x
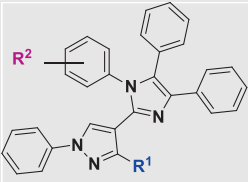
Sr. No.	R^1	R^2	Product	Time (min)	Yield[b] (%)	m.p. (°C)	Lit m.p. (°C) (Ref)
1	Ph	H	**5a**	30	82	200–202	194 (Shirole et al. 2017)
2	Ph	*para*-Cl	**5b**	45	75	215–217	214 (Shirole et al. 2017)
3	Ph	*para*-Br	**5c**	45	72	180–182	–
4	Ph	*para*-OCH$_3$	**5d**	30	80	156–158	–
5	Ph	3,5-(CH$_3$)$_2$	**5e**	30	71	102–104	–
6	Biph	*meta*-Cl	**5f**	60	77	158–160	–
7	Biph	*para*-Cl	**5g**	60	75	200–202	–
8	Biph	*para*-Br	**5h**	60	78	218–220	–
9	Biph	*para*-OCH$_3$	**5i**	45	82	186–187	–
10	Biph	3,5-(CH$_3$)$_2$	**5j**	45	73	164–166	–
11	*para*-ClPh	*para*-Br	**5k**	30	82	218–220	220 (Chaudhry et al. 2019)
12	*para*-ClPh	*para*-OCH$_3$	**5l**	30	85	200–201	202 (Chaudhry et al. 2019)
13	*para*-ClPh	3,5-(CH$_3$)$_2$	**5m**	45	88	170–172	170 (Chaudhry et al. 2019)
14	*para*-BrPh	*para*-Cl	**5n**	45	80	194–196	194 (Chaudhry et al. 2019), 198 (Shirole et al. 2017)
15	*para*-BrPh	*para*-OCH$_3$	**5o**	45	86	200–202	200 (Chaudhry et al. 2019)
16	*para*-BrPh	3,5-(CH$_3$)$_2$	**5p**	45	90	168–170	168 (Chaudhry et al. 2019)
17	*para*-OCH$_3$Ph	*para*-OCH$_3$	**5q**	30	85	178–180	180 (Chaudhry et al. 2019)
18	*para*-OCH$_3$Ph	3,5-(CH$_3$)$_2$	**5r**	30	88	173–174	172 (Chaudhry et al. 2019)
19	*meta*-NO$_2$Ph	*para*-OCH$_3$	**5s**	45	90	214–216	214 (Chaudhry et al. 2019)
20	*meta*-NO$_2$Ph	3,5-(CH$_3$)$_2$	**5t**	45	92	158–160	158 (Chaudhry et al. 2019)
21	Coumarinyl	*para*-Cl	**5u**	90	85	204–206	205 (Chaudhry et al. 2017c)
22	Coumarinyl	*para*-Br	**5v**	90	82	260–262	260 (Chaudhry et al. 2017c)
23	Coumarinyl	*para*-OCH$_3$	**5w**	60	80	238–240	238 (Chaudhry et al. 2017c)
24	Coumarinyl	3,5-(CH$_3$)$_2$	**5x**	60	86	210–212	210 (Chaudhry et al. 2017c)

[a] Reaction condition: pyrazole-3-carbaldehydes **1a-1g** (1 mmol), anilines **2a-2f** (1 mmol), benzil **3** (1 mmol), ammonium acetate **4** (1 mmol), glutamic acid (15 mol %), refluxed in EtOH.

[b] Isolated yields.

20 mol% catalyst dose also gave comparable results. Different solvents were also selected while searching out for the most suitable conditions. Out of six solvents, two solvents MeOH and EtOH were upended to be as the best choice. The reaction completion time was the same with the slight difference in product yield (Table 1).

Considering the reaction completion times, calculated yields, and as a simple convenient approach; refluxing of MCR mixture with 15 % glutamic acid in EtOH was preferred for further preparations of **5b-5x**. The scope of current reaction approach is evident in Table 2, wherein, the optimized conditions were applied in the MCRs of different substituted anilines and other aldehydic precursors also. The novel products of the series, **5c-5j** were characterized with the help of physical and spectral records. Initially FTIR spectra were taken and there was no residual band observed for the precursor's functional groups which indicated the complete conversion of reactants into their respective products. There was no absorption band detected in N—H region which supported the plausible formation of *N*-substituted imidazoles. Absorption bands of the finger-print region were also in accordance with the designed molecular structures of **5c-5j**.

All ^{1}H NMR and ^{13}C NMR spectra (**5c-5j**) had proton and carbon-13 signals at their appropriate positions as well. NMR spectra of the derivative **5c** (as a representative analogue) are shown in Fig. 2. The H-5 of pyrazole appeared downfield as a singlet at δ 8.34 ppm. Two doublets were spotted with J value 8.5 Hz for the protons of *para*-Br substituted phenyl ring (Ar^3) at δ 6.33 ppm and δ 6.97 ppm. Other phenyl protons appeared in the aromatic region around δ 7.0 ppm to δ 8.0 ppm. In ^{13}C NMR, two most important signals were observed, one of quaternary C-2 imidazole detected at δ 140.55 ppm while second significant signal of linking C-4 of pyrazole found near to δ 112.19 ppm.

Considering the expected stability associated with such bulky aryl- and heteroaryl- tethered molecules, the molecular ion peaks (M$^+$) were detected as base peaks in MS data of nearly all derivatives (**5c-5j**). The expulsion of halogens (M$^+$−Cl and/or M$^+$−Br) was observed in halogenated molecules (**5c, 5f, 5g,** and **5h**). A characteristic stable fragment of m/z 165 was also found in all cases which probably produced through skeletal rearrangement of an unstable intermediate fragment (Chaudhry, et al. 2021; Compernolle and Dekeirel 1971). Identification of probable key fragments in the mass
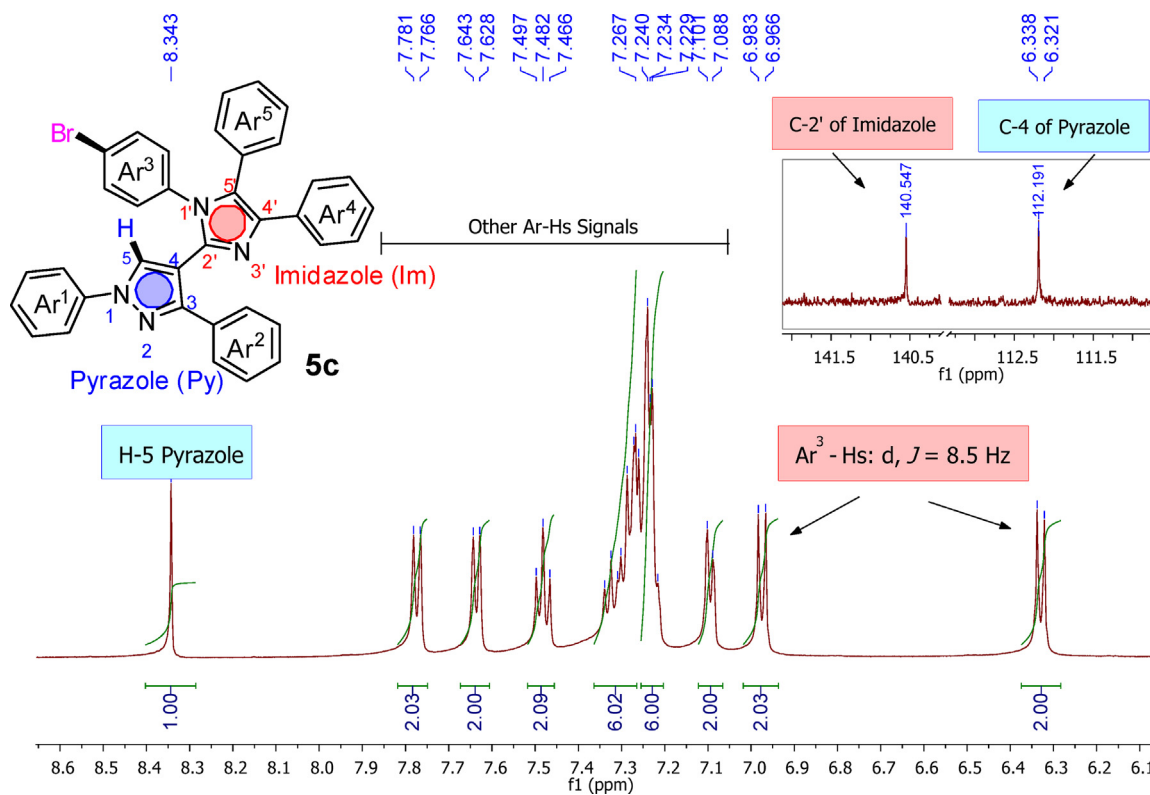
Fig. 2 Characteristics signals in ^{1}H NMR and ^{13}C NMR spectra of novel derivative (**5c**) as a representative analogue.
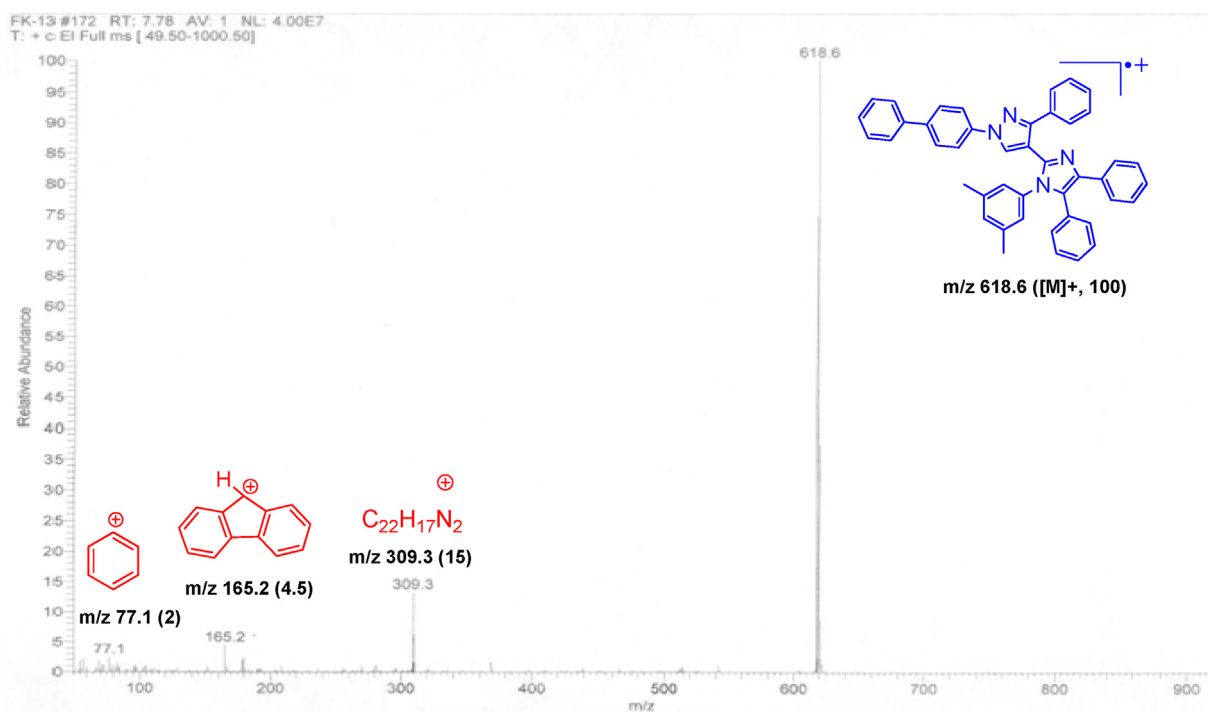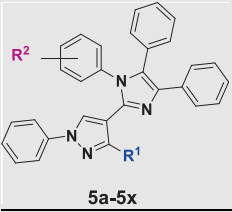

Fig. 3 Characteristics mass spectrum of novel derivative (**5j**) as a representative analogue.

Table 3 AChE and BChE inhibitory profiles of compounds (**5a-5x**), Mean ± SEM, n = 3.

5a-5x

SrNo.	Compound	R^1	R^2	AChE IC_{50} (μM)	BChE IC_{50} (μM)	Selectivity Index (SI)	
						AChE[a]	BChE[b]
1	**5a**	Ph	H	41.27 ± 0.56	0.35 ± 0.02	0.01	117.91
2	**5b**	Ph	para-Cl	36.82 ± 0.45	7.82 ± 0.12	0.21	4.71
3	**5c**	Ph	para-Br	71.46 ± 0.62	8.43 ± 0.11	0.12	8.48
4	**5d**	Ph	para-OCH$_3$	142.91 ± 0.49	138.21 ± 0.22	0.97	1.03
5	**5e**	Ph	3,5-(CH$_3$)$_2$	175.28 ± 0.75	9.75 ± 0.13	0.06	17.98
6	**5f**	Biph	meta-Cl	312.53 ± 0.82	9.84 ± 0.11	0.03	31.76
7	**5g**	Biph	para-Cl	332.91 ± 0.93	> 500	–	–
8	**5h**	Biph	para-Br	354.26 ± 0.87	> 500	–	–
9	**5i**	Biph	para-OCH$_3$	132.68 ± 0.56	136.91 ± 0.25	1.03	0.97
10	**5j**	Biph	3,5-(CH$_3$)$_2$	116.35 ± 0.54	21.43 ± 0.14	0.18	5.43
11	**5k**	para-ClPh	para-Br	78.52 ± 0.47	333.44 ± 0.2	4.25	0.24
12	**5l**	para-ClPh	para-OCH$_3$	135.46 ± 0.49	147.16 ± 0.25	1.09	0.92
13	**5m**	para-ClPh	3,5-(CH$_3$)$_2$	41.36 ± 0.36	5.73 ± 0.09	0.14	7.22
14	**5n**	para-BrPh	para-Cl	192.32 ± 0.53	> 500	–	–
15	**5o**	para-BrPh	para-OCH$_3$	35.19 ± 0.42	235.34 ± 0.15	6.69	0.15
16	**5p**	para-BrPh	3,5-(CH$_3$)$_2$	63.27 ± 0.56	3.60 ± 0.12	0.06	17.58
17	**5q**	para-OCH$_3$Ph	para-OCH$_3$	62.75 ± 0.52	> 500	–	–
18	**5r**	para-OCH$_3$Ph	3,5-(CH$_3$)$_2$	34.12 ± 0.35	> 500	–	–
19	**5s**	meta-NO$_2$Ph	para-OCH$_3$	342.62 ± 0.85	> 500	–	–
20	**5t**	meta-NO$_2$Ph	3,5-(CH$_3$)$_2$	36.25 ± 0.37	142.00 ± 0.18	3.92	0.26
21	**5u**	Coumarinyl	para-Cl	64.12 ± 0.28	24.94 ± 0.21	0.39	2.57
22	**5v**	Coumarinyl	para-Br	437.52 ± 0.87	19.62 ± 0.15	0.04	22.30
23	**5w**	Coumarinyl	para-OCH$_3$	35.61 ± 0.36	14.93 ± 0.09	0.42	2.39
24	**5x**	Coumarinyl	3,5-(CH$_3$)$_2$	25.83 ± 0.25	7.64 ± 0.13	0.30	3.38
25	**Eserine**	–	–	0.19 ± 0.06	0.62 ± 0.08	3.26	0.31

[a] Selectivity for AChE = IC_{50} (BChE) / IC_{50} (AChE).
[b] Selectivity for BChE = IC_{50} (AChE) / IC_{50} (BChE).

5a

AChE IC_{50} (μM) = 41.27±0.56
BChE IC_{50} (μM) = 0.35±0.02
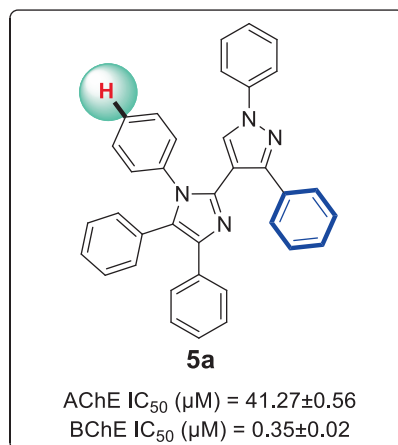
Fig. 4 Structure of the most potent and highly selective BChE inhibitor (**5a**) of the series.

spectrum of representative **5j** is presented in Fig. 3. Elemental CHN-analyses also confirmed the synthesis and isolation of pure products.

3.2. AChE and BChE inhibitory activities with SAR studies

Herein, these heteroaryl substituted imidazoles (**5a-5x**) were further investigated for their *in vitro* AChE and BChE inhibition activity in the quest of new and potent AChE and BChE inhibitors (Table 3). The most potent BChE inhibitory activity was displayed by the simplest molecule **5a** of the series with IC_{50} 0.35 ± 0.02 μM in contrast with the reference drug eserine (0.62 ± 0.08 μM) (**Fig. 32S**). The calculated SI value 117.91 is highlighting the high selectivity of this compound for BChE inhibition over AChE enzyme inhibition (Fig. 4).

The region A and region B of the main template were further modified with different substitutions to examine the overall SAR (Fig. 7). A *para*-Cl derivative **5b** and *para*-Br derivative **5c** also showed potent BChE inhibition with IC_{50}
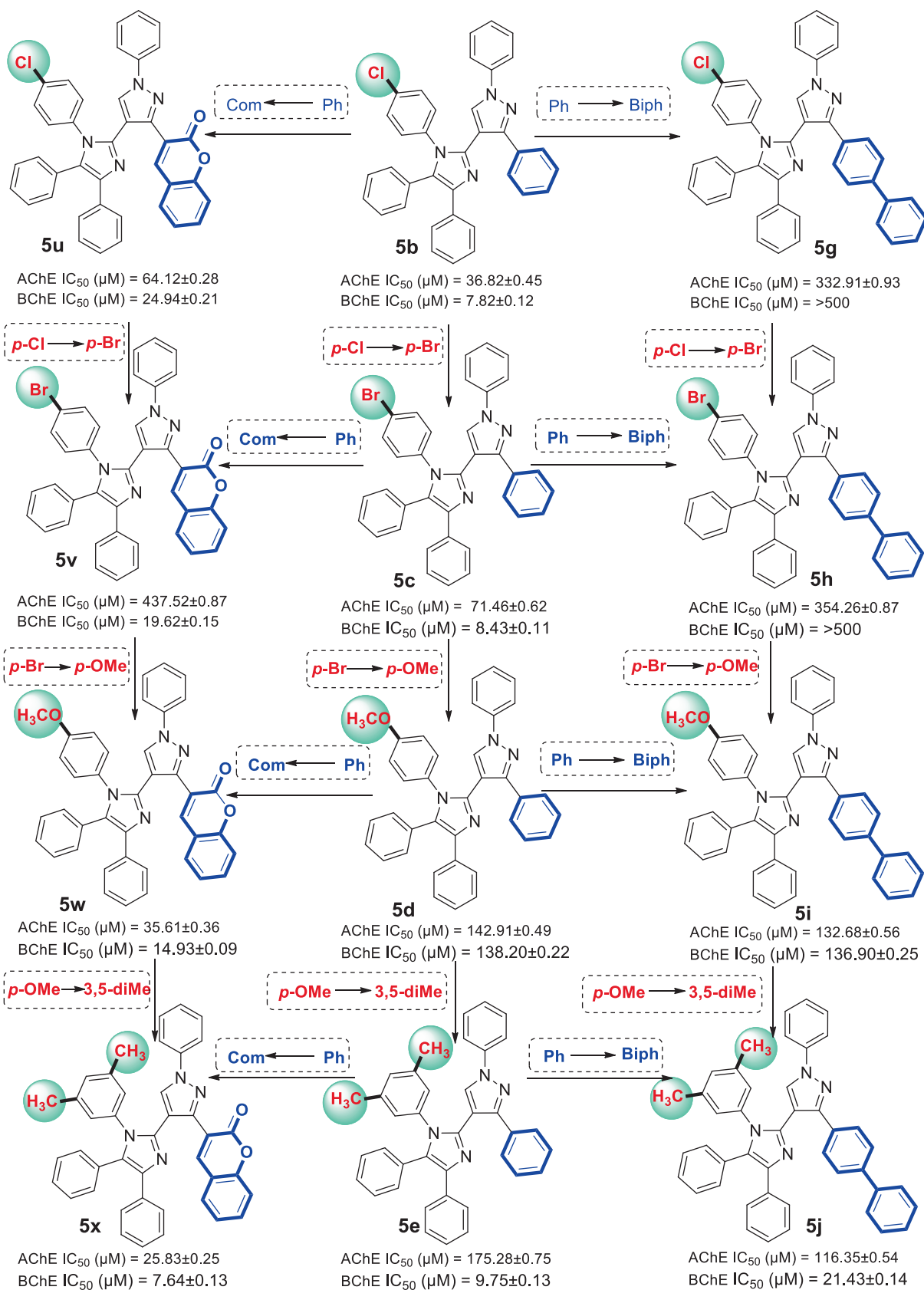
5u

AChE IC$_{50}$ (μM) = 64.12±0.28
BChE IC$_{50}$ (μM) = 24.94±0.21

5b

AChE IC$_{50}$ (μM) = 36.82±0.45
BChE IC$_{50}$ (μM) = 7.82±0.12

5g

AChE IC$_{50}$ (μM) = 332.91±0.93
BChE IC$_{50}$ (μM) = >500

5v

AChE IC$_{50}$ (μM) = 437.52±0.87
BChE IC$_{50}$ (μM) = 19.62±0.15

5c

AChE IC$_{50}$ (μM) = 71.46±0.62
BChE IC$_{50}$ (μM) = 8.43±0.11

5h

AChE IC$_{50}$ (μM) = 354.26±0.87
BChE IC$_{50}$ (μM) = >500

5w

AChE IC$_{50}$ (μM) = 35.61±0.36
BChE IC$_{50}$ (μM) = 14.93±0.09

5d

AChE IC$_{50}$ (μM) = 142.91±0.49
BChE IC$_{50}$ (μM) = 138.20±0.22

5i

AChE IC$_{50}$ (μM) = 132.68±0.56
BChE IC$_{50}$ (μM) = 136.90±0.25

5x

AChE IC$_{50}$ (μM) = 25.83±0.25
BChE IC$_{50}$ (μM) = 7.64±0.13

5e

AChE IC$_{50}$ (μM) = 175.28±0.75
BChE IC$_{50}$ (μM) = 9.75±0.13

5j

AChE IC$_{50}$ (μM) = 116.35±0.54
BChE IC$_{50}$ (μM) = 21.43±0.14

Fig. 5   Variation in AChE and BChE inhibitions with structural modifications in the compounds: **5b-5e**, **5 g-5j** and **5u-5x**.
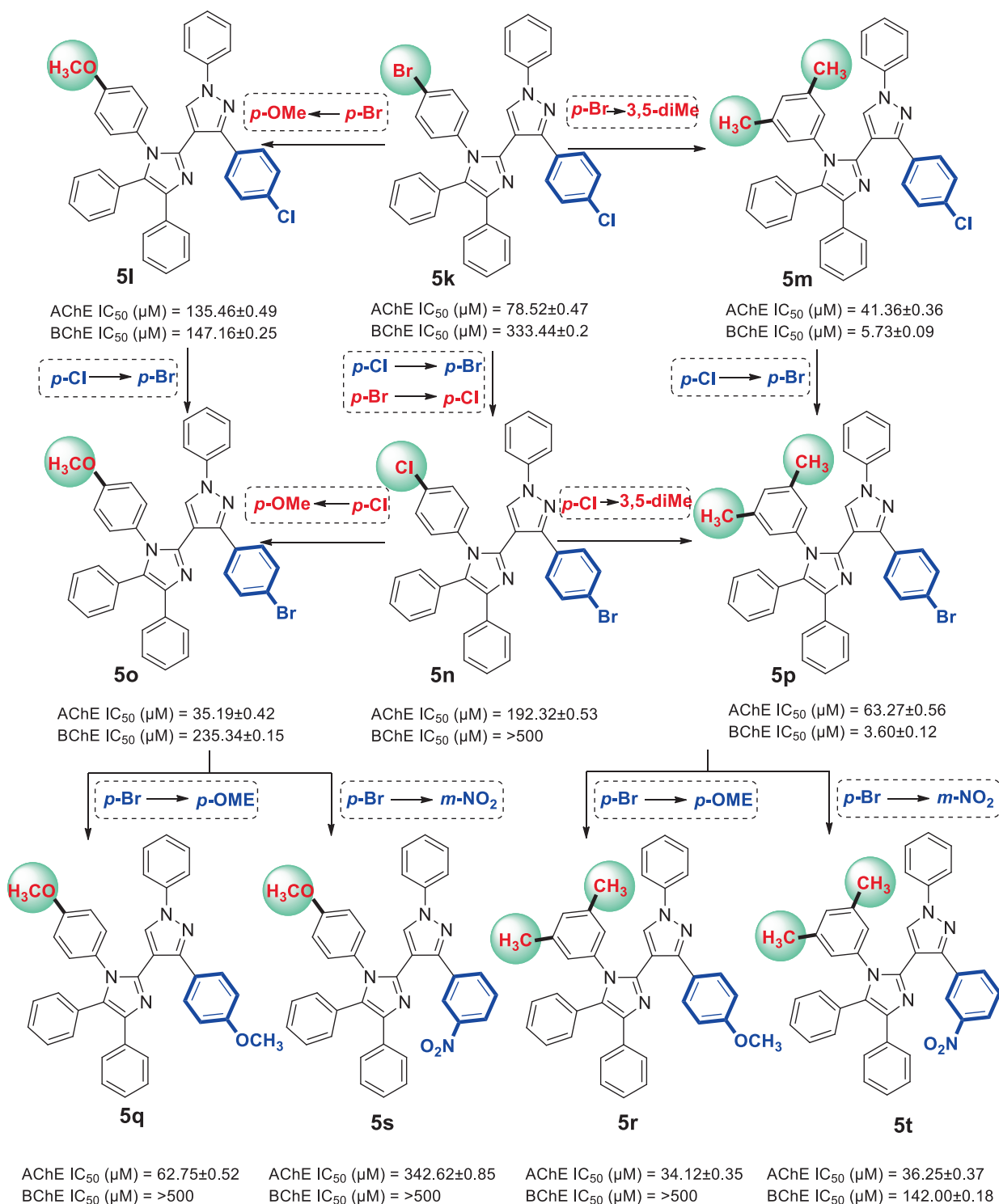
Fig. 6 Variation in AChE and BChE inhibitions with structural modifications in the compounds: 5 k-5 t.

7.82 ± 0.12 μM and IC$_{50}$ 8.43 ± 0.11 μM respectively. On the other side, **5b** and **5c** exhibited moderate AChE inhibitory activity. It is reported that methoxy group substituted structural frameworks are good cholinesterase inhibitors (Gao et al. 2021). However, in the present case, insertion of methoxy group at the *para* position in compound **5d** had no significant improvement in the ChEs inhibition profile (AChE IC$_{50}$ 142. 91 ± 0.49 μM and BChE IC$_{50}$ 138.21 ± 0.22 μM). Substitution of two hydrophobic methyl groups in *N*-aryl ring of imidazole (**5e**) led to strong in BChE inhibitory activity with IC$_{50}$ 9.75 ± 0.13 μM (SI for BChE = 17.98) (Fig. 4) (Larik et al. 2020).

Overall effects of R² functionalities on the activity:

- Halogens (Cl or Br) have increased BChE inhibition (**5b**, **5c**, and **5f**)
- *para*-OCH₃ substitution enhances the AChE inhibitng potency in few compounds **5o** and **5w** due to probable synergistic effects of region A and region B
- 3,5-Dimethyl substitution has overall excellent results disclosing hydrophobicity as important controlling factor
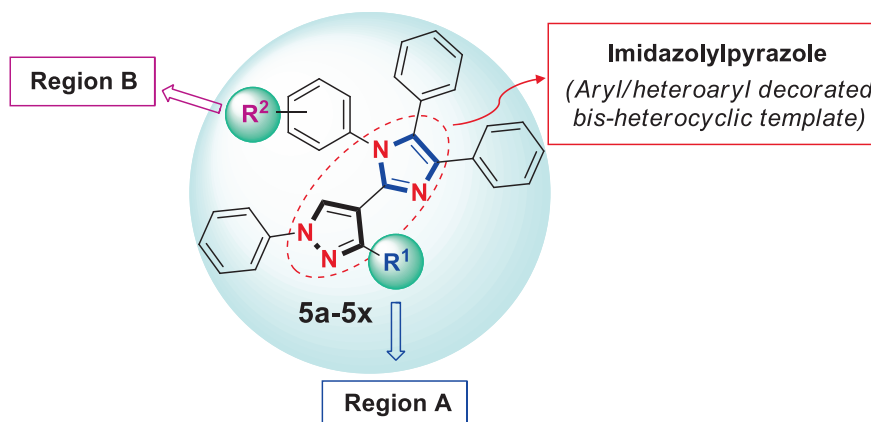
Probable Effects of different R¹ substitutions on the ChEs inihibition:

- A simple phenyl ring at this position results in highly effective & selective BChE inhibition (**5a**)
- *para*-Cl or *para*-Br substituted phenyl rings have moderate to excellent effects on the ChEs inhibition depending upon the nature of substituents in the region B
- *para*-OCH₃ substituted phenyl ring significantly improves the AChE inhibition while results in loss of BChE inhibiting potential
- *para*-NO₂ substitution in the phenyl ring increases AChE inhibition through hydrogen bonding, however, could not improve the BChE inhibiting potential
- Switching of phenyl to a bulky biphenyl moiety decreases the inhibiting potentials
- Coumarinyl moiety at this position significantly improves the overall ChEs inhibition

Fig. 7   The summarized SAR of heteroaryl substituted imidazole derivatives (**5a-5x**).
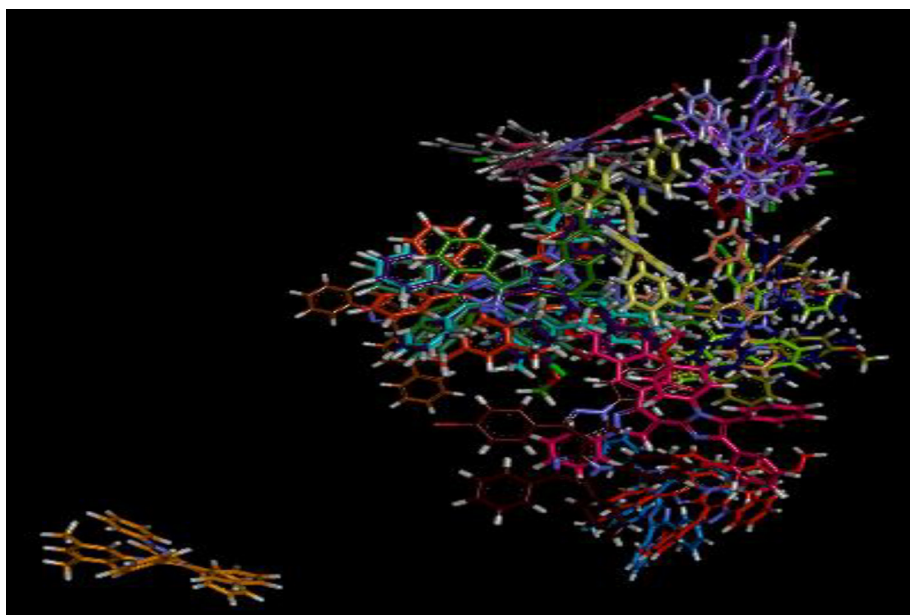

Fig. 8   Overlap of bound complexes of compounds (**5a-5x**) showing overlap in the hotspot **5a** (grey), **5b** (pink), **5c** (yellow magenta), **5d** (beige), **5e** (mustard), **5f** (baby pink), **5g** (purple), **5h** (brown), **5i** (green), **5j** (orange), **5k** (parrot green), **5l** (olive green), **5m** (mauve), **5n** (reddish brown), **5o** (chocolate brown), **5p** (pearly purple), **5q** (ink blue), **5r** (navy blue), **5s** (dirty green), **5t** (red), **5u** (dark purple), **5v** (see green), **5w** (shocking pink), **5x** (sky blue) and eserine (black).
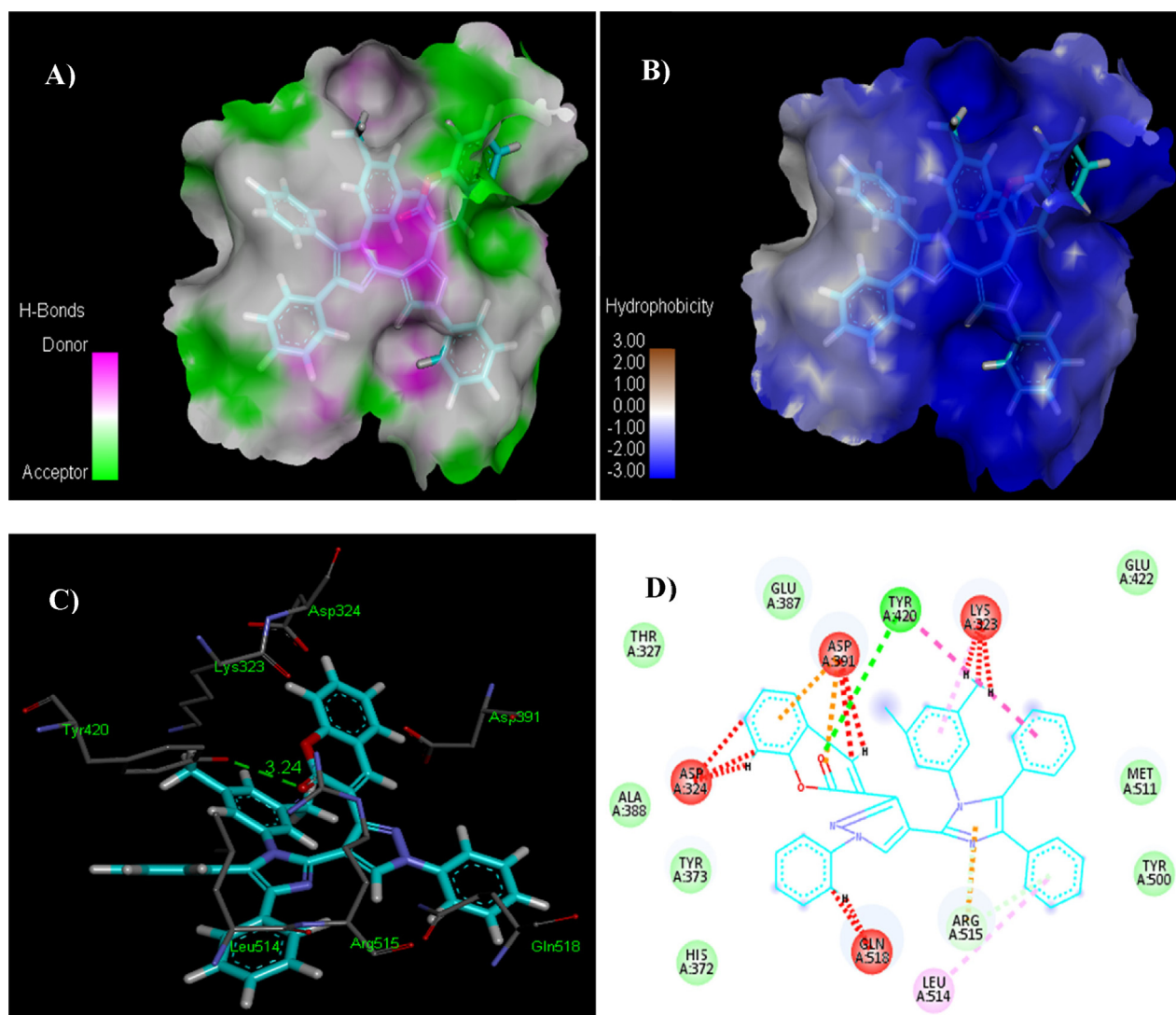
Fig. 9 The analyses illustrating H-bonds (A) and hydrophobic contacts (B) of compound **5x**. In the hydrophobic interactions (right) the blue color demonstrates favorable structural features (atoms and torsions) donating to the total binding energy within the AChE hotspot (PDB ID: 4m0e), the pink corresponds to unfavorable, and the white is neutral one. Fig. 9C is 3D and Fig. 9D is 2D depictions of docked ligand **5x**.

Wang *et al.* documented biphenyl derivatives as good ChEs inhibitors (Wang et al. 2017). On the contrary, in the present studies, extending the phenyl to bulky biphenyl group reduced the ChEs inhibitory activity. Substitution of electron withdrawing halogen functionalities did not display much positive influence on inhibitory profile. It has been observed that *meta*-Cl derivative **5f** is 31.76 folds more selective BChE inhibitor with IC$_{50}$ 9.84 $\pm$ 0.11 μM. However, the placement of Cl from *meta* to *para* position as in **5g** (IC$_{50}$ > 500 μM against BChE, IC$_{50}$ 332.91 $\pm$ 0.93 μM against AChE), leads to complete loss of inhibitory activity (Rehuman et al. 2021). It is therefore proposed that the positioning of substituents affects the enzyme inhibitory activity of the compounds and even may result in the loss of activity. A *para*-Br analogue **5h** was also found inactive because of the same reason. On the other hand, replace-ment of halogen with methoxy group as noticed in **5i**, slightly improved the inhibitory activity while the substitution of 3,5-dimethyl in **5j** significantly enhanced the inhibition of both enzymes (AChE IC$_{50}$ 116.35 $\pm$ 0.54 μM and BChE IC$_{50}$ 21.43 $\pm$ 0.14 μM) (Fig. 5).

ChEs inhibition was much improved by the introduction of coumarin moiety in the molecular framework (**5u-5x**) as observed in another study (Rehuman et al. 2021). The AChE and BChE IC$_{50}$ values of *para*-Cl derivative **5u** are 64.12 $\pm$ 0.28 μM and 24.94 $\pm$ 0.21 μM respectively. Surprisingly, the AChE inhibition by *para*-Br derivative **5v** was less than of anti-BChE activity with 22.30 folds selectivity for BChE over AChE. Though presence of electron donating methoxy group in compound **5w** displayed better inhibition but switching to 3,5-dimethyl substitution has significantly
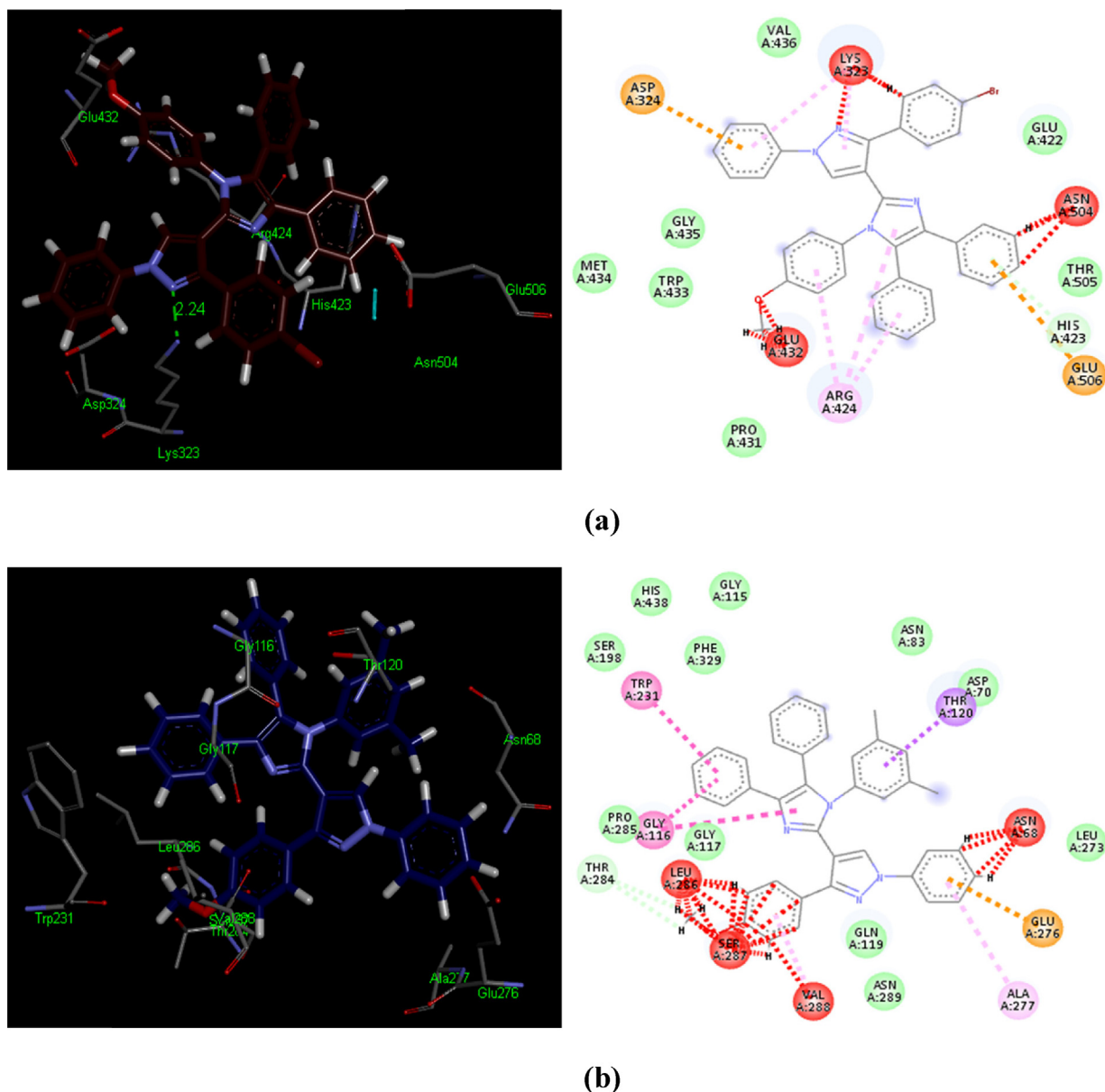
(a)

(b)

Fig. 10   3D and 2D depictions of docked ligands − **5o (a)** and **5r (b):** demonstrating unfavorable bump (red), π-cation (brown), π-alkyl (light pink), amide π-stack (pink) and π-π *T*-shaped (shocking pink) contacts inside a hotspot of the AChE (PDB ID: 4M0E).

enhanced the ChEs inhibitory potentials, thus, **5x** was found out to be the best AChE inhibitor of the series with IC_{50} 25.83 ± 0.25 μM (Fig. 5). A dihalogenated derivative **5k** displayed moderate AChE inhibition (IC_{50} 78.52 ± 0.47 μM) but poor BChE inhibitory activity (IC_{50} 333.44 ± 0.2 μM). Swapping the halogens such as *para*-Cl with *para*-Br substitutions in **5n** did not confer better outcomes. However, some interesting variations were observed with further modifications in the substitutions. When *para*-Br functionality was replaced with *para*-OMe group (**5l**), its BChE inhibiting activity was slightly improved to IC_{50} 147.16 ± 0.25 μM. However, by doing so there was a decline in the AChE inhibition (IC_{50} 135.46 ± 0.49 μM). Comparable trend was found in **5o** derivative with BChE (IC_{50} 235.34 ± 0.15 μM), while there was a

significant increase in AChE inhibition (IC_{50} 35.19 ± 0.42 μM) with selectivity of 6.69 over BChE. The replacement of halogens with hydrophobic dimethyl substitutions has significantly increased the anti-cholinesterase activity in derivative **5m** (AChE IC_{50} 41.36 ± 0.36 μM and BChE IC_{50} 5.73 ± 0.09 μM) and derivative **5p** (AChE IC_{50} 63.27 ± 0.56 μM and BChE IC_{50} 3.60 ± 0.12 μM). Three methoxy analogues (**5q-5s**) of the series were inactive against BChE. On the contrary, derivatives **5q** and **5r** have displayed good anti-AChE activity IC_{50} 62.75 ± 0.52 μM and IC_{50} 34.12 ± 0.35 μM. A *meta*-NO_2 derivative (**5t**) possessing dimethyl functionalities is also found to be a good AChE inhibitor (IC_{50} 36.25 ± 0.37 μM) due to possible hydrogen bonding of –NO_2 group with amino acids (Fig. 6).

Table 4 Binding contacts of compounds (**5a-5x**) to AChE protein (PDB ID 4M0E) using *PatchDock*.

| Compound	Score	ACE (kcal/mol)	Hydrogen bond interactions	Distance (Å)	Hydrophobic interactions	π-π T-shaped interactions
5a	6016	−378.78	–	–	Trp231, Ala232, Ala229, Trp522, Pro527, Pro401, Thr523, Glu404, Asn228, Leu307, Phe227, Pro303, Val294	–
5b	5976	−312.87	–	–	Asp304, Pro303, Met302, Ser235, Thr234, Val361, Val529, Phe526, Phe526, Tyr396, Pro527, Trp522, Thr523, Cys400, Glu404, Asn228	–
5c	6832	−334.87	–	–	Asn384, Gln380, Thr374, Gln518, Ala388	Trp376, Tyr373, Tyr373, His372
5d	6190	−367.34	–	–	Pro285, Asn289, Glu276, Gln119, Asp70, Gly117, His438, Ser198, Ala199, Phe329, Asn397	Trp231, Gly116
5e	5980	−334.56	–	–	Val136, Glu137, Lys476, Tyr477, Asn473, Ser487, Ile462, Ser466	–
5f	6878	−421.54	–	–	Asn289, Val288, Pro359, Tyr396, Phe358, Phe526, Ser362, Tyr237, Asn241	Tyr282
5g	6678	−389.67	–	–	Phe357, Asn397, Pro230, Phe358, Ser362	Tyr396
5h	6679	−355.89	Gln176	2.18	Asn181, Lys9, Trp177, Tyr33, Gln47, Pro46, Asp297, Phe298	–
5i	6490	−400.54	–	–	Val436, Glu422, Met511, Leu514, Tyr500, His372, Tyr373, Ala388, Arg386, Gly390, Thr327, Asp324	Lys323
5j	6567	−367.44	–	–	Thr327, Gly390, Glu387, Thr374, Lys513, Leu514, Tyr500, Glu422	Tyr373
5k	6467	−423.90	–	–	Glu276, Asn289, Gln119, Pro285, Gly117, Phe329, Phe398, Ala199, His438, Gly115, Trp82	Trp231
5l	6467	−378.45	–	–	Asn289, Val288, Gly117, Ser198, Ala199, Gly115, Glu197, Pro84, Ser79, Asn83, Asp70	Trp82
5m	6856	−400.45	–	–	Asn289, Glu238, Asn241, Phe526, Phe358, Tyr396, Phe357, Val288	Val361
5n	6489	−378.56	–	–	Val393, Asn397, Phe357, Tyr396, Phe526, Ser287, Asn289, Thr284	Phe358
5o	7346	−341.21	–	–	Val436, Glu422, Thr505, Pro431, Trp433, Gly435, Met434	Arg424
5p	711.90	−345.90	–	–	Val361, Val529, Phe526, Tyr396, Pro527, Trp522, Cys400, Thr523, Glu404, Asp304, Asn228, Ala232, Ser235, Thr234	–
5q	6367	−378.34	–	–	Ala62, Tyr61, Asn57, Asp54, Asp91, Ser89, Asp87	–
5r	7411	−311.09	–	–	Ser198, His438, Gly115, Phe329, Asn83, Asp70, Leu273, Asn289, Gln119, Gly117, Pro285	Trp231, Gly116
5s	6056	−323.45	Thr59, Lys60	3.25, 1.34	Ser89, Asp91, Tyr94, Trp56, Asn57, Ala58, Gly30, Leu29	–
5t	6589	−300.45	Thr59, Lys60	3.25, 1.34	Ser89, Asp91, Tyr94, Trp56, Asn57, Ala58, Gly30, Leu29	–
5u	6789	−356.23	Tyr420	3.13	His372, Tyr373, Trp376, Ala388, Gly435, Glu387, Tyr500	–
5v	6789	−312.34	–	–	His372, Tyr373, Ala388, Glu387, Thr327, Asp324, Lys323, Glu422, Met511, Tyr500	–
5w	6456	412.67	–	–	Asn342, Asp391, Arg515, Gly435, Glu422, His423, Arg381, Glu383	–
5x	7564	−291.90	Tyr420	3.24	Thr327, Glu387, Glu422, Met511, Tyr500, His372, Tyr373, Ala388	–
Eserine (Std.)	4826	−183.17	Tyr124	2.78	Glu202, Ser203, Phe238, Phe395, Phe297, Arg296, Trp286, Asp74, Trp86, Gly121	Tyr341
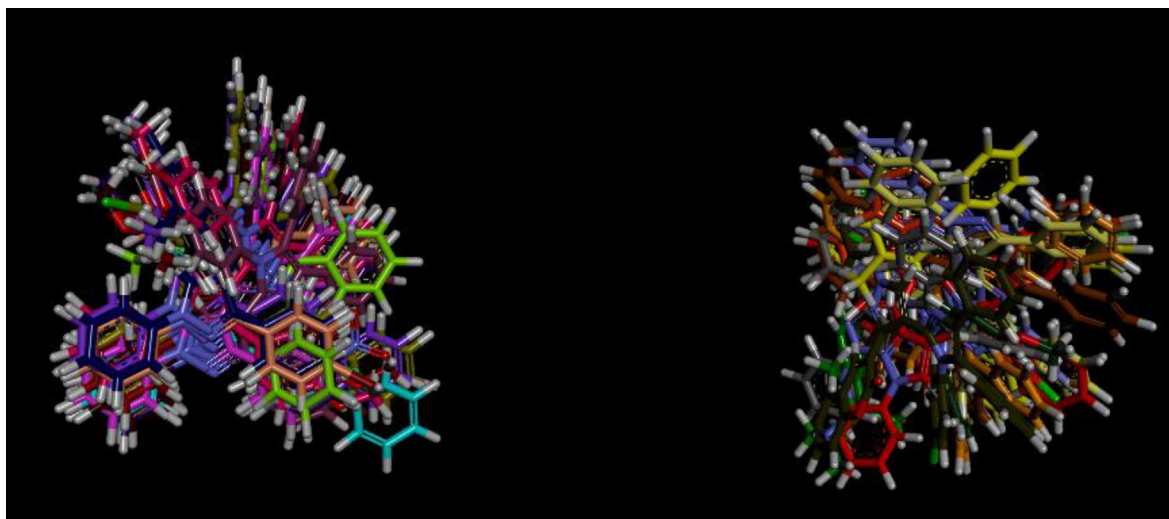
Fig. 11 Overlap of bound conformations of compounds **5a-5j** showing overlap in two clusters in the binding pocket **5a** (grey), **5b** (lemon yellow), **5c** (magenta), **5d** (pearly purple), **5e** (parrot green), **5f** (brown), **5g** (dirty green), **5h** (sky blue), **5i** (mustard), **5j** (purple), **5k** (mauve), **5 l** (chocolate brown), **5m** (navy blue), **5n** (orange), **5o** (black), **5p** (beige), **5q** (shocking pink), **5r** (reddish brown), **5s** (baby pink), **5t** (dark purple), **5u** (olive green), **5v** (red), **5w** (dark green), **5x** (yellow) and eserine (green).

This general SAR model concludes that such aryl and/or heteroaryl decorated imidazole derivatives **(5a-5x)** appear to be a new potent class of ChEs inhibitors wherein the nature and bulkiness of the substituents greatly influenced the binding of the ligand with the target enzyme (Fig. 7). Overall selectivity data facilitates in identifying three selective AChE inhibitors of the series (**5k**, **5o**, and **5t**) and five highly selective BChE inhibitors of the series (**5a**, **5e**, **5f**, **5p**, and **5v**) (Table 3). Nevertheless, *in silico* molecular docking investigations helped to further understand the significant ligand-enzyme interactions in correlation with these *in vitro* findings.

3.3. Molecular docking studies

3.3.1. AChE docking calculations

The docked conformations of compounds (**5a-5x**) were examined in order to evaluate the qualitative estimation and the recognition of molecular basis of the analyzed biological activities (IC_{50}), as shown in Fig. 8. In the preliminary evaluation of the docked complexes of AChE, it was revealed that all compounds (**5a-5x**) showed considerable contact patterns (Table S1).

Compound **5x** exhibited the most potent contact with AChE with a score of 7564 and an ACE of –291.90 kcal/mol. The interacting residues of this complex are His372, Tyr373, Ala388, Glu387, Glu422, Met511, Tyr500, Pro527, Thr327 and Gly117. Ligand **5x** has shown hydrogen bonding with Tyr420. The length of hydrogen bond was 3.24 Å. Compound **5x** also exhibited hydrophobic interaction potential with pocket amino acids Thr327, Glu387, Glu422, Met511, Tyr500, His372, Tyr373 and Ala388 residues (Fig. 9).

Interestingly, other two best ligands **5o** and **5r** exhibited no hydrogen bond contact with AChE receptor but instead found considerable geometric fit of these compounds in the receptor and therefore scoring in *PatchDock* being based on shape com-

plementarity principles, it revealed a score of 7346 and 7411 and ACE values –341.21 and –311.09 kcal/mol respectively in the docked interactions with the AChE enzyme. Compound **5o** and **5r** have shown π-π T-shaped contacts with Arg424 and Trp231, Gly116 accordingly (Fig. 10). Compound **5t** has shown two hydrogen bond contacts with hydroxyl group of Thr59 and oxygen of NO_2 functionality with an average distance of 3.25 Å. Similarly, another hydrogen bonding was observed between amino of Lys60 and oxygen of NO_2 group (1.34 Å). Compound **5t** revealed hydrophobic contact potential with amino acid residues Ser89, Asp91, Tyr94, Trp56, Asn57, Ala58, Gly30 and Leu29 (Table S1). Other potent compounds such as **5a, 5b, 5m** and **5w** illustrated hydrophobic contact potential with AChE receptor amino acids and compound **5m** has exhibited π-π T-shaped contact with Val361 (Table S1). However, our docking evaluations have suggested that compounds **5o**, **5r** and **5x** for AChE revealed the significant inhibitory potential against AChE and these outcomes are consistent with the IC_{50} values of these ligands. The conformational poses of all structures (**5a-5x**) are demonstrating the maximal biological activities with their constructive contacts in the binding hotspots (Table 4).

3.3.2. BChE docking calculations

The qualitative assessment and the recognition of molecular basis of the calculated BChE inhibitory activity (IC_{50}), the docked conformations of compounds (**5a-5x**) were examined as shown in Fig. 11.

In the preliminary evaluation of the docked complexes of BChE, it was revealed that all compounds (**5a-5x**) showed significant interaction patterns (Table S2). Compound **5a** exhibited the most potent contact with BChE with a score of 7096 and an ACE of –332.95 kcal/mol. The interacting residues of this complex are Phe398, Gly116, Ala388, Asp391, Gln518, Phe371, Asn384, Arg381, Glu387, Tyr373, Trp82, Trp231
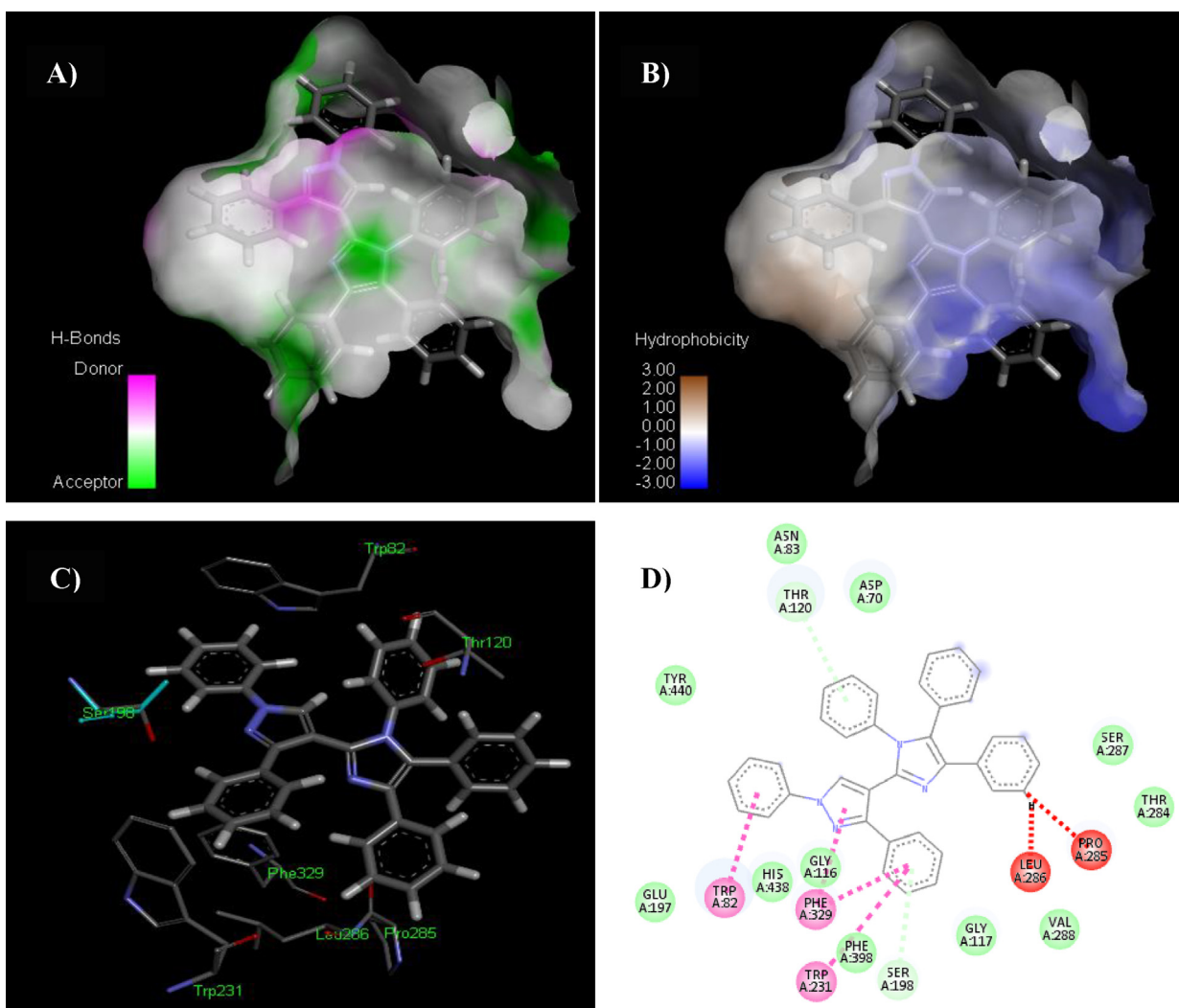
Fig. 12   The analyses showing H-bonds (A) and hydrophobic contacts (B) of compound **5a**. In the hydrophobic contacts (right) the blue color shows favorable structural features (atoms and torsions) donating to the whole binding energy inside the BChE binding pouch (PDB ID: 4bds), the pink representing unfavorable, and the white is neutral one. Fig. 12-**C** is 3D and Fig. 12-**D** is 2D representations of docked ligand **5a**.

and Trp376 (Fig. 12). Compound **5a** exhibited hydrophobic interaction potential with pocket amino acids Tyr440, Asn83, Asp70, Ser287, Thr284, Val288, Gly117, Phe398, Gly116, His438, Glu197 residues and also illustrated π-π *T*-shaped contact potential with Trp82, Phe329, Trp231 amino acid residues. Interestingly, best two ligands **5a** and **5m** exhibited no hydrogen bond contact with BChE receptor but instead found considerable geometric fit of these compounds in the receptor and therefore scoring in *PatchDock* being based on shape complementarity principles. The compound **5m** revealed a score of 6998 and ACE value –404.36kcal/mol in the docked interactions with the BChE enzyme. Ligand **5p** has shown a hydrogen bond interaction with amino group of Ala388 and bromo of 4–bromophenyl moiety with an average distance of

3.02 Å. Compounds **5m** and **5p** depicted hydrophobic interaction potential with BChE receptor amino acids Ala388, Glu387, Arg381, Asn384, Gln384, Thr374 and Glu387, Thr374, Gln380, Asp395, Phe371 respectively. Compound **5m** and **5p** has formed π-π *T*-shaped interaction with Tyr373, Tyr373, Trp376 and Tyr373, Tyr373, Trp376 correspondingly (Fig. 13).

Resultantly, our docking calculations have proposed that compounds **5a**, **5m** and **5p** for BChE exhibited the excellent inhibitory potential against BChE and these results are consistent with the IC_{50} values of these compounds. The conformational orientations of all compounds **(5a-5x)** are demonstrating the maximal biological activities with their favorable interactions in the binding pouches (Table 5).
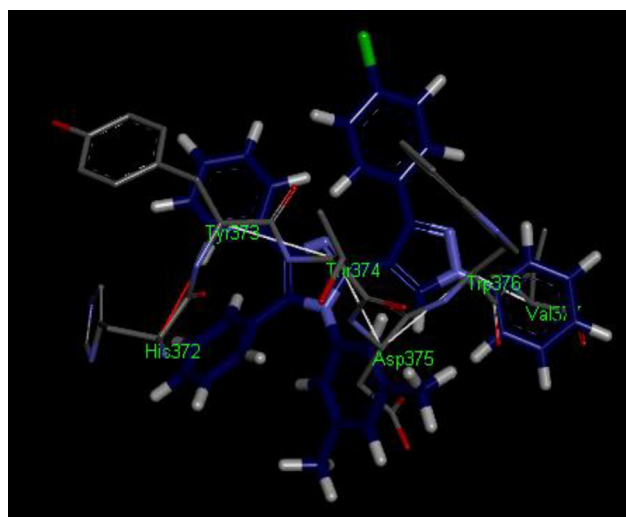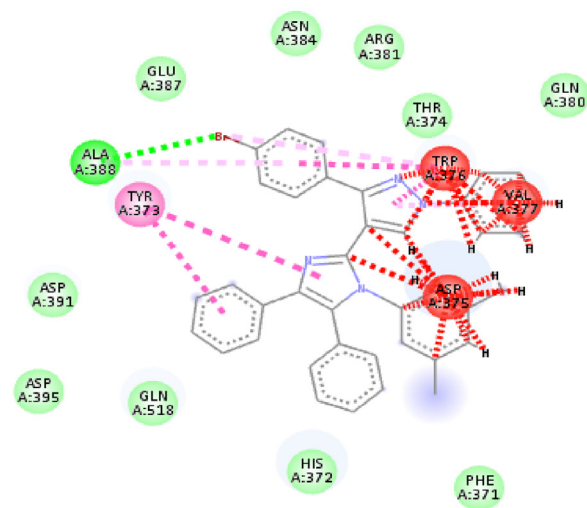
(a)
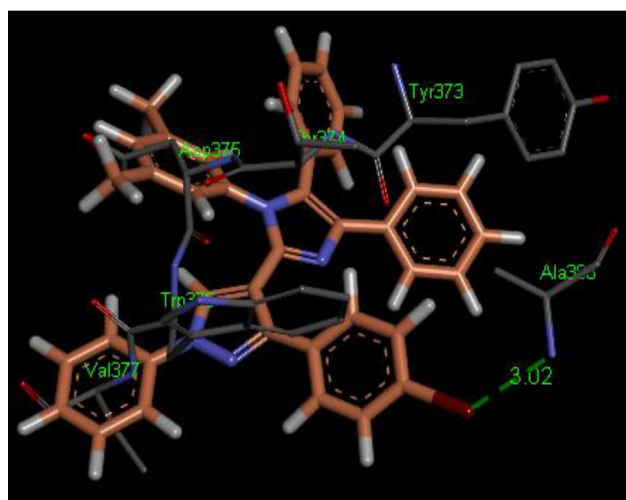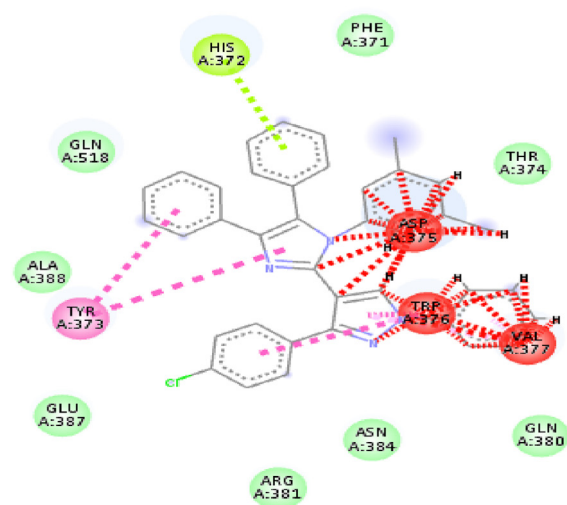
(b)

Fig. 13   3D and 2D depictions of docked ligands – **5m (a)** and **5p (b):** demonstrating H-bond (light green), unfavorable bump (red), π-alkyl (light pink), amide π-stack (pink) and π-π *T*-shaped (shocking pink) contacts inside a binding pouch of the BChE (PDB ID: 4BDS).

Table 5 Binding interactions of compounds (5a-5x) to BChE protein (PDB ID: 4bds) using *PatchDock*.

Compound	Score	ACE (kcal/mol)	Hydrogen bond interactions	Distance (Å)	Hydrophobic interactions	π-π T-shaped interactions
5a	7096	−332.95	–	–	Tyr440, Asn83, Asp70, Ser287, Thr284, Val288, Gly117, Phe398, Gly116, His438, Glu197	Trp82, Phe329, Trp231
5b	6978	−345.85	–	–	Gly127, Ser198, Phe398, Gly116, Trp82, Asn83, Asp70, Asn68, Glu276, Asn289, Gln119, Val288	–
5c	6940	−356.56	–	–	Ala388, Asp391, Gln518, Phe371, Thr374, Asn384, Arg381, Glu387	Tyr373
5d	5870	−363.06	–	–	Phe371, Thr374, Asn384, Glu387, Ala388, Asp391, Asp395	Tyr332
5e	5862	−311.73	–	–	Gln380, Arg381, ASn384, Glu383, Glu387, Ala388, Asp391, Tyr373, Asp395, Gln518, His372	Trp376
5f	6472	−457.04	–	–	Asp70, Asn83, Gly116, Thr120, Pro285, Thr284, Asn397, Gly117, Phe398, Gly115, Glu197	Trp82, Trp231
5g	6576	−378.61	–	–	Thr374, His372, Gln518, Ala388, Tyr373, Glu387, Arg381	Trp376
5h	6474	−348.11	–	–	Asn384, Arg381, Glu383, Asp391, Ala388, Gln518, Phe371, Thr374	Trp376
5i	6998	−414.34	–	–	Ser79, Asn83, Glu276, Asn289, Ser287, Gln119, Gly117, Val288, Phe398, Asn397, His438, Ile442	Trp231
5j	6462	−362.67	–	–	Gln380, Arg381, Glu387, Tyr373, Ala388, Gln518, His372, Phe371, Thr374	Trp376
5k	6320	−410.48	–	–	Thr284, Ser189, His438, Gly115, Asn83, Glu276	–
5l	6038	−357.18	–	–	Ala388, Thr374, Phe371	Tyr373
5m	6998	−404.36	–	–	Ala388, Glu387, Arg381, Asn384, Gln384, Thr374	Tyr373, Tyr373, Trp376
5n	6386	−369.44	–	–	Thr284, Glu276, Phe398, Ala199, His438, Gly115,	Trp231, Phe329, Gly116, Gly116
5o	6156	−297.92	–	–	Thr374, Phe371, Ala388, Asp391	Tyr373, Trp376
5p	7029	−356.84	Ala388	3.02	Glu387, Thr374, Gln380, Asp395, Phe371	Tyr373, Tyr373, Trp376
5q	6192	−389.06	–	–	Gln380, Ala388, Arg380, Thr374	Tyr373, Tyr373, Trp376
5r	6028	−336.77	–	–	Arg515, Phe371, Thr374, Ala388	Tyr373, Trp376, Trp376
5s	6198	−314.69	–	–	Phe371, Ala388, Thr374	Tyr373, Trp376
5t	6288	−312.13	–	–	Phe371, Ala388, Thr374	Tyr373, Trp376
5u	6408	−388.41	–	–	Phe398, Tyr440, Met437, Ser79	Phe329, Trp231
5v	6198	−336.65	–	–	Gly78, Met437, Tyr440, Ser79, Asn83, Phe398, Phe118	Trp231
5w	6348	400.51	–	–	Glu197, Gly115, Ala199, Asn397, Asn83, Ser79, Tyr332, Glu276	Gly116, Trp82
5x	6252	−520.40	–	–	Glu276, Leu273, Ala199, Thr284, Asn83, Phe389, His438	Gly116, Trp231
Eserine	4462	170.03	Tyr128	3.35	Leu125, Ile442, Glu197, Phe329, Tyr332, Trp430, Ser79, Tyr440, Met437, Gly78	Trp82

4. Conclusion

A series of heteroaryl substituted imidazoles (5a-5x) was synthesized and screened against AChE and BChE to evaluate their inhibitory potential in search of leads in the treatment of AD. At first, the synthetic reaction conditions were optimized by using different amino acids as catalysts, and polar / non-polar solvents. The facile and efficient synthetic methodology was adopted to prepare target series in excellent yields by employing the glutamic acid as a useful catalyst. The novel derivatives were further characterized through FTIR, EI-MS, ^{1}H NMR, ^{13}C NMR and CHN analyses. These compounds were further tested against both AChE and BChE enzymes. It is concluded from SAR results that imidazole is a core moiety and the aryl/heteroaryl rings along with structural modifications in the region-A and region-B are strongly correlated with enzyme inhibitions. A coumarinyl moiety containing imidazolylpyrazole derivative 5x was the most active AChE enzyme inhibitor with IC$_{50}$ 25.83 $\pm$ 0.25 μM. While a simple phenyl decorated imidazolylpyrazole scaffold 5a was the most potent BChE inhibitor with IC$_{50}$ 0.35 $\pm$ 0.02 μM when compared to standard eserine (BChE IC$_{50}$ 0.62 $\pm$ 0.08 μM). This molecule also has SI of 117.91 for BChE. Docking simulation disclosed the strong hydrophobic and π-π T-shaped interactions of 5a with the enzyme though hydrogen bonding was not involved in the enzyme inhibitor complex. Other potent BChE inhibitors of the series are 5p, 5m, 5x, 5b, 5c, 5e and 5f with IC$_{50}$ values from 3.60 $\pm$ 0.12 μM to 9.84 $\pm$ 0. 11 μM. Moreover, molecular docking studies of all the synthesized compounds have depicted critical interaction patterns with AChE and BChE enzymes and are in complete agreement with the *in vitro* findings. Hence, this study highlights some hopeful structural features for further studies in detail wherein potent compounds could be employed in new drug discovery.

Declaration of Competing Interest

The authors declare that they have no known competing financial interests or personal relationships that could have appeared to influence the work reported in this paper.

Acknowledgment

Appendix A. Supplementary material

Supplementary data to this article can be found online at https://doi.org/10.1016/j.arabjc.2022.104384.

References

Abdel-Wahab, B.F., Khidre, R.E., Farahat, A.A., 2011. Pyrazole-3(4)-carbaldehyde: synthesis, reactions and biological activity. ARKIVOC I, 196–245. https://doi.org/10.3998/ark.5550190.0012.103.

Alghamdi, S.S., Suliman, R.S., Almutairi, K., Kahtani, K., Aljatli, D., 2021. Imidazole as a promising medicinal scaffold: current status and future direction. Drug Des. Devel. Ther. 15, 3289–3319. https://doi.org/10.2147/DDDT.S307113.

Almansour, A.I., Arumugam, N., Kumar, R.S., Kotresha, D., Manohar, T.S., Venketesh, S., 2020. Design, synthesis and cholinesterase inhibitory activity of novel spiropyrrolidine tethered imidazole heterocyclic hybrids. Bioorg. Med. Chem. Lett. 30, (2). https://doi.org/10.1016/j.bmcl.2019.126789 126789.

Athar, T., Al Balushi, K., Khan, S.A., 2021. Recent advances on drug development and emerging therapeutic agents for Alzheimer's disease. Mol. Biol. Rep. 48 (7), 5629–5645. https://doi.org/10.1007/s11033-021-06512-9.

Benazzouz-Touami, A., Chouh, A., Halit, S., Terrachet-Bouaziz, S., Makhloufi-Chebli, M., Ighil-Ahriz, K., Silva, A.M., 2022. New coumarin-pyrazole hybrids: synthesis, docking studies and biological evaluation as potential cholinesterase inhibitors. J. Mol. Struct. 1249,. https://doi.org/10.1016/j.molstruc.2021.131591 131591.

Chatonnet, A., Lockridge, O., 1989. Comparison of butyryl-cholinesterase and acetylcholinesterase. Biochem. J. 260 (3), 625–634. https://doi.org/10.1042/bj2600625.

Chaudhry, F., Naureen, S., Ijaz, F., Munawar, M.A., Khan, M.A., 2017a. Amino acid catalyzed reactions. a facile route to some heteroarylbispyrazoles. Synth. Commun. 47 (4), 310–318. https://doi.org/10.1080/00397911.2016.1263336.

Chaudhry, F., Naureen, S., Huma, R., Shaukat, A., Al-Rashida, M., Asif, N., Ashraf, M., Munawar, M.A., Khan, M.A., 2017b. In search of new α-glucosidase inhibitors: imidazolylpyrazole derivatives. Bioorg. Chem. 71, 102–109. https://doi.org/10.1016/j.bioorg.2017.01.017.

Chaudhry, F., Choudhry, S., Huma, R., Ashraf, M., Al-Rashida, M., Munir, R., Sohail, R., Jahan, B., Munawar, M.A., Khan, M.A., 2017c. Hetarylcoumarins: synthesis and biological evaluation as potent α-glucosidase inhibitors. Bioorg. Chem. 73, 1–9. https://doi.org/10.1016/j.bioorg.2017.05.009.

Chaudhry, F., Naureen, S., Ashraf, M., Al-Rashida, M., Jahan, B., Munawar, M.A., Khan, M.A., 2019. Imidazole-pyrazole hybrids: synthesis, characterization and in-vitro bioevaluation against α-glucosidase enzyme with molecular docking studies. Bioorg. Chem. 82, 267–273. https://doi.org/10.1016/j.bioorg.2018.10.047.

Chaudhry, F., Shahid, W., Al-Rashida, M., Ashraf, M., Munawar, M. A., Khan, M.A., 2021. Synthesis of imidazole-pyrazole conjugates bearing aryl spacer and exploring their enzyme inhibition poten-

tials. Bioorg. Chem. 108,. https://doi.org/10.1016/j.bioorg.2021.104686 104686.

Cheung, J., Gary, E.N., Shiomi, K., Rosenberry, T.L., 2013. Structures of human acetylcholinesterase bound to dihydrotanshinone I and territrem B show peripheral site flexibility. ACS Med. Chem. Lett. 4 (11), 1091–1096. https://doi.org/10.1021/ml400304w.

Compernolle, F., Dekeirel, M., 1971. Nitrogen elimination in the mass spectra of diphenyl and triphenyl-v-triazoles. Org. Mass Spectrom. 5 (4), 427–436. https://doi.org/10.1002/oms.1210050408.

Cummings, J., Lee, G., Nahed, P., Kambar, M.E.Z.N., Zhong, K., Fonseca, J., Taghva, K., 2022. Alzheimer's disease drug development pipeline 2022. Alzheimer's Dement. Transl. Res. Clin. Interv. 8 (1), e12295. https://doi.org/10.1002/trc2.12295.

da Costa, J.S., Lopes, J.P.B., Russowsky, D., Petzhold, C.L., de Amorim Borges, A.C., Ceschi, M.A., Konrath, E., Batassini, C., Lunardi, P.S., Gonçalves, C.A.S., 2013. Synthesis of tacrine-lophine hybrids via one-pot four component reaction and biological evaluation as acetyl-and butyrylcholinesterase inhibitors. Eur. J. Med. Chem. 62, 556–563. https://doi.org/10.1016/j.ejmech.2013.01.029.

Darvesh, S., 2016. Butyrylcholinesterase as a diagnostic and therapeutic target for Alzheimer's disease. Curr. Alzheimer Res. 13 (10), 1173–1177. https://doi.org/10.2174/1567205013666160404120542.

Derabli, C., Boualia, I., Abdelwahab, A.B., Boulcina, R., Bensouici, C., Kirsch, G., Debache, A., 2018. A cascade synthesis, in vitro cholinesterases inhibitory activity and docking studies of novel tacrine-pyranopyrazole derivatives. Bioorg. Med. Chem. Lett. 28 (14), 2481–2484. https://doi.org/10.1016/j.bmcl.2018.05.063.

Dhingra, A.K., Chopra, B., Jain, A., Chaudhary, J., 2022. Imidazole: multi-targeted therapeutic leads for the management of Alzheimer's disease. Mini-Rev. Med. Chem. 22 (10), 1352–1373. https://doi.org/10.2174/1389557522666220104152141.

Fernández-Bolaños, J.G., López, Ó., 2022. Butyrylcholinesterase inhibitors as potential anti-Alzheimer's agents: an updated patent review (2018-present). Expert Opin. Ther. Pat. 32 (8), 913–932. https://doi.org/10.1080/13543776.2022.2083956.

Gao, H., Jiang, Y., Zhan, J., Sun, Y., 2021. Pharmacophore-based drug design of AChE and BChE dual inhibitors as potential anti-Alzheimer's disease agents. Bioorg. Chem. 114,. https://doi.org/10.1016/j.bioorg.2021.105149 105149.

Gaugler, J., James, B., Johnson, T., Reimer, J., Solis, M., Weuve, J., Buckley, R.F., Hohman, T.J., 2022. 2022 Alzheimer's disease facts and figures. Alzheimer's Dement. 18 (4), 700–789. https://doi.org/10.1002/alz.12638.

Grutzendler, J., Morris, J.C., 2001. Cholinesterase inhibitors for Alzheimer's disease. Drugs 61 (1), 41–52. https://doi.org/10.2165/00003495-200161010-00005.

Jing, L., Wu, G., Kang, D., Zhou, Z., Song, Y., Liu, X., Zhan, P., 2019. Contemporary medicinal-chemistry strategies for the discovery of selective butyrylcholinesterase inhibitors. Drug Discov. 24 (2), 629–635. https://doi.org/10.1016/j.drudis.2018.11.012.

Jun, J., Baek, J., Yang, S., Moon, H., Kim, H., Cho, H., Hah, J.M., 2021. Discovery of a potent and selective JNK3 inhibitor with neuroprotective effect against amyloid β-induced neurotoxicity in primary rat neurons. Int. J. Mol. Sci. 22 (20), 11084. https://doi.org/10.3390/ijms222011084.

Kabir, M.T., Uddin, M., Begum, M., Thangapandiyan, S., Rahman, M., Aleya, L., Mathew, B., Ahmed, M., Barreto, G.E., Ashraf, G. M., 2019. Cholinesterase inhibitors for Alzheimer's disease: multitargeting strategy based on anti-Alzheimer's drugs repositioning. Curr. Pharm. Des. 25 (33), 3519–3535. https://doi.org/10.2174/1381612825666191008103141.

Karlsson, D., Fallarero, A., Brunhofer, G., Guzik, P., Prinz, M., Holzgrabe, U., Erker, T., Vuorela, P., 2012. Identification and characterization of diarylimidazoles as hybrid inhibitors of butyrylcholinesterase and amyloid beta fibril formation. Eur. J. Pharm. Sci. 45 (1–2), 169–183. https://doi.org/10.1016/j.ejps.2011.11.004.

Kaur, M., Priya, A., Sharma, A., Singh, A., Banerjee, B., 2022. Glycine and its derivatives catalyzed one-pot multicomponent synthesis of bioactive heterocycles. Synth. Commun. 1–22. https://doi.org/10.1080/00397911.2022.2090262.

Kumari, S., Maddeboina, K., Bachu, R.D., Boddu, S.H., Trippier, P. C., Tiwari, A.K., 2022. Pivotal role of nitrogen heterocycles in Alzheimer's disease drug discovery. Drug Discov. 27, (10). https://doi.org/10.1016/j.drudis.2022.07.007 103322.

Kuzu, B., Tan, M., Taslimi, P., Gülçin, İ., Taşpınar, M., Menges, N., 2019. Mono-or di-substituted imidazole derivatives for inhibition of acetylcholine and butyrylcholine esterases. Bioorg. Chem. 86, 187–196. https://doi.org/10.1016/j.bioorg.2019.01.044.

Larik, F.A., Saeed, A., Faisal, M., Hamdani, S., Jabeen, F., Channar, P.A., Mumtaz, A., Khan, I., Kazi, M.A., Abbas, Q., Hassan, M., 2020. Synthesis, inhibition studies against AChE and BChE, drug-like profiling, kinetic analysis and molecular docking studies of N-(4-phenyl-3-aroyl-2(3H)-ylidene) substituted acetamides. J. Mol. Struct. 1203,. https://doi.org/10.1016/j.molstruc.2019.127459 127459.

Li, M., Dong, Y., Yu, X., Li, Y., Zou, Y., Zheng, Y., He, Z., Liu, Z., Quan, J., Bu, X., Wu, H., 2017a. Synthesis and evaluation of diphenyl conjugated imidazole derivatives as potential glutaminyl cyclase inhibitors for treatment of Alzheimer's disease. J. Med. Chem. 60 (15), 6664–6677. https://doi.org/10.1021/acs.jmedchem.7b00648.

Li, Q., Yang, H., Chen, Y., Sun, H., 2017b. Recent progress in the identification of selective butyrylcholinesterase inhibitors for Alzheimer's disease. Eur. J. Med. Chem. 132, 294–309. https://doi.org/10.1016/j.ejmech.2017.03.062.

Li, Q., Chen, Y., Xing, S., Liao, Q., Xiong, B., Wang, Y., Lu, W., He, S., Feng, F., Liu, W., Chen, Y., 2021. Highly potent and selective butyrylcholinesterase inhibitors for cognitive improvement and neuroprotection. J. Med. Chem. 64 (10), 6856–6876. https://doi.org/10.1021/acs.jmedchem.1c00167.

Lott, I.T., Head, E., 2019. Dementia in Down syndrome: unique insights for Alzheimer disease research. Nat. Rev. Neurol. 15 (3), 135–147. https://doi.org/10.1038/s41582-018-0132-6.

Ma, W., Bi, J., Zhao, C., Gao, Y., Zhang, G., 2020. Design, synthesis and biological evaluation of acridone glycosides as selective BChE inhibitors. Carbohydr. Res. 491,. https://doi.org/10.1016/j.carres.2020.107977 107977.

Mlakić, M., Odak, I., Faraho, I., Talić, S., Bosnar, M., Lasić, K., Barić, D., Škorić, I., 2022. New naphtho/thienobenzo-triazoles with interconnected anti-inflammatory and cholinesterase inhibitory activity. Eur J. Med. Chem. 241,. https://doi.org/10.1016/j.ejmech.2022.114616 114616.

Nachon, F., Carletti, E., Ronco, C., Trovaslet, M., Nicolet, Y., Jean, L., Renard, P.Y., 2013. Crystal structures of human cholinesterases in complex with huprine W and tacrine: elements of specificity for anti-Alzheimer's drugs targeting acetyl- and butyryl-cholinesterase. Biochem. J. 453 (3), 393–399. https://doi.org/10.1042/BJ20130013.

Naureen, S., Ijaz, F., Nazeer, A., Chaudhry, F., Munawar, M.A., Khan, M.A., 2017. Facile, eco-friendly, one-pot protocol for the synthesis of indole-imidazole derivatives catalyzed by amino acids. Synth. Commun. 47 (16), 1478–1484. https://doi.org/10.1080/00397911.2017.1332766.

Nguyen, T.T., Le, N.P.T., Tran, P.H., 2019. An efficient multicomponent synthesis of 2,4,5-trisubstituted and 1,2,4,5-tetrasubstituted imidazoles catalyzed by a magnetic nanoparticle supported Lewis acidic deep eutectic solvent. RSC Adv. 9 (65), 38148–38153. https://doi.org/10.1039/C9RA08074K.

Obaid, R.J., Naeem, N., Mughal, E.U., Al-Rooqi, M.M., Sadiq, A., Jassas, R.S., Moussa, Z., Ahmed, S.A., 2022. Inhibitory potential of nitrogen, oxygen and sulfur containing heterocyclic scaffolds against acetylcholinesterase and butyrylcholinesterase. RSC Adv. 12 (31), 19764–19855. https://doi.org/10.1039/d2ra03081k.

Porsteinsson, A.P., Isaacson, R.S., Knox, S., Sabbagh, M.N., Rubino, I., 2021. Diagnosis of early alzheimer's disease: clinical practice in 2021. J. Prev. Alzheimer's Dis. 8 (3), 371–386. https://doi.org/10.14283/jpad.2021.23.

Purgatorio, R., de Candia, M., Catto, M., Carrieri, A., Pisani, L., De Palma, A., Toma, M., Ivanova, O.A., Voskressensky, L.G., Altomare, C.D., 2019. Investigating 1,2,3, 4,5,6-hexahydroazepino [4,3-b] indole as scaffold of butyrylcholinesterase-selective inhibitors with additional neuroprotective activities for Alzheimer's disease. Eur. J. Med. Chem. 177, 414–424. https://doi.org/10.1016/j.ejmech.2019.05.062.

Qin, P., Ran, Y., Liu, Y., Wei, C., Luan, X., Niu, H., Peng, J., Sun, J., Wu, J., 2022. Recent advances of small molecule JNK3 inhibitors for Alzheimer's disease. Bioorg. Chem. 128,. https://doi.org/10.1016/j.bioorg.2022.106090 106090.

Ramrao, S.P., Verma, A., Waiker, D.K., Tripathi, P.N., Shrivastava, S.K., 2021. Design, synthesis, and evaluation of some novel biphenyl imidazole derivatives for the treatment of Alzheimer's disease. J. Mol. Struct. 1246,. https://doi.org/10.1016/j.molstruc.2021.131152 131152.

Rehuman, N.A., Oh, J.M., Nath, L.R., Khames, A., Abdelgawad, M. A., Gambacorta, N., Nicolotti, O., Jat, R.K., Kim, H., Mathew, B., 2021. Halogenated coumarin–chalcones as multifunctional monoamine oxidase-B and butyrylcholinesterase inhibitors. ACS Omega 6 (42), 28182–28193. https://doi.org/10.1021/acsomega.1c04252.

Rosenberry, T.L., Brazzolotto, X., Macdonald, I.R., Wandhammer, M., Trovaslet-Leroy, M., Darvesh, S., Nachon, F., 2017. Comparison of the binding of reversible inhibitors to human butyrylcholinesterase and acetylcholinesterase: a crystallographic, kinetic and calorimetric study. Molecules 22 (12), 2098. https://doi.org/10.3390/molecules22122098.

Rossi, R., Angelici, G., Casotti, G., Manzini, C., Lessi, M., 2019. Catalytic synthesis of 1,2,4,5-tetrasubstituted 1H-imidazole derivatives: state of the art. Adv. Synth. Catal. 361 (12), 2737–2803. https://doi.org/10.1002/adsc.201801381.

Sari, S., Akkaya, D., Zengin, M., Sabuncuoğlu, S., Özdemir, Z., Alagöz, M.A., Karakurt, A. and Barut, B., 2022. Antifungal azole derivatives featuring naphthalene prove potent and competitive cholinesterase inhibitors with potential CNS penetration according to the in vitro and in silico studies. Chem. Biodivers. 19 (7), e202200027. https://doi.org/10.1002/cbdv.202200027.

Schneidman-Duhovny, D., Inbar, Y., Nussinov, R., Wolfson, H.J., 2005. PatchDock and SymmDock: servers for rigid and symmetric docking, Nucleic Acids Res. 33 (suppl_2), W363-W367. https://doi.org/10.1093/nar/gki481.

Shirole, G.D., Kadnor, V.A., Tambe, A.S., Shelke, S.N., 2017. Brønsted-acidic ionic liquid: green protocol for synthesis of novel tetrasubstituted imidazole derivatives under microwave irradiation via multicomponent strategy. Res. Chem. Intermed. 43 (2), 1089–1098. https://doi.org/10.1007/s11164-016-2684-7.

Takeda, A., Okai, H., Watabe, K., Iida, H., 2022. Metal-free atomeconomical synthesis of tetra-substituted imidazoles via flaviniodine catalyzed aerobic cross-dehydrogenative coupling of amidines and chalcones. J. Org. Chem. 87 (15), 10372–10376. https://doi.org/10.1021/acs.joc.2c00596.

Tariq, S., Mutahir, S., Khan, M.A., Mutahir, Z., Hussain, S., Ashraf, M., Bao, X., Zhou, B., Stark, C.B., Khan, I.U., 2022. Synthesis, in vitro cholinesterase inhibition, molecular docking, DFT and ADME studies of novel 1,3,4-oxadiazole-2-thiol derivatives. Chem. Biodiversity 19, e202200157.

Tripathi, A., Choubey, P.K., Sharma, P., Seth, A., Saraf, P., Shrivastava, S.K., 2020. Design, synthesis, and biological evaluation of ferulic acid based 1,3,4-oxadiazole hybrids as multifunctional therapeutics for the treatment of Alzheimer's disease. Bioorg. Chem. 95,. https://doi.org/10.1016/j.bioorg.2019.103506 103506.

Vachan, B.S., Karuppasamy, M., Vinoth, P., Vivek Kumar, S., Perumal, S., Sridharan, V., Menéndez, J.C., 2020. Proline and its derivatives as organocatalysts for multi-component reactions in aqueous media: synergic pathways to the green synthesis of heterocycles. Adv. Synth. Catal. 362 (1), 87–110. https://doi.org/10.1002/adsc.201900558.

Vijverberg, E.G.B., Axelsen, T.M., Bihlet, A.R., Henriksen, K., Weber, F., Fuchs, K., Harrison, J.E., Kühn-Wache, K., Alexandersen, P., Prins, N.D., Scheltens, P., 2021. Rationale and study design of a randomized, placebo-controlled, double-blind phase 2b trial to evaluate efficacy, safety, and tolerability of an oral glutaminyl cyclase inhibitor varoglutamstat (PQ912) in study participants with MCI and mild AD-VIVIAD. Alzheimer's Res. Ther. 13 (1), 1–8. https://doi.org/10.1186/s13195-021-00882-9.

Wang, D.M., Feng, B., Fu, H., Liu, A.L., Wang, L., Du, G.H., Wu, S., 2017. Design, synthesis, and biological evaluation of a new series of biphenyl/bibenzyl derivatives functioning as dual inhibitors of acetylcholinesterase and butyrylcholinesterase. Molecules 22 (1), 172. https://doi.org/10.3390/molecules22010172.